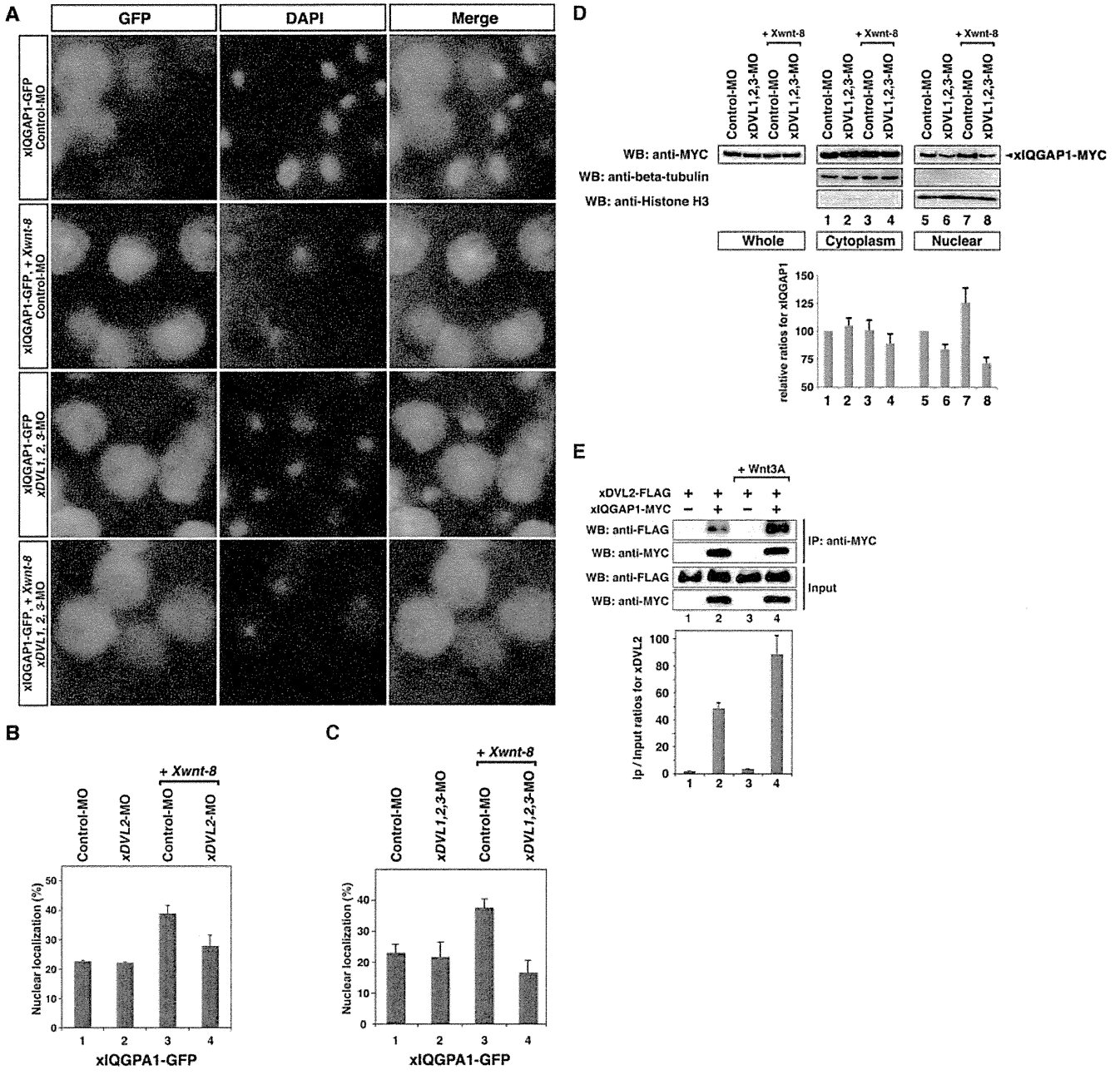

Figure 3. Localization of xIQGAP1-GFP. (**A**) Nuclear localization of xIQGAP1-GFP in stage 10 *Xenopus* animal cap cells over-expressing *Xwnt-8* and *xDVL1, 2, 3*-MO. GFP signals (left). DAPI staining of animal cap cells (center). Merge (right). (**B, C**)The ratio of cells that had nuclear fluorescence signals. The following procedure is indicated in Figure 2C. (**B**) The ratio of nuclear localized xIQGAP1-GFP in cells injected with *xDVL2*-MO. Lane 1: n = 388, 22.7%, lane 2: n = 361, 22.2%, lane 3: n = 616, 20.9%, lane 4: n = 534, 39.7%. $P>0.1$ [between lane 1 and lane 2], $P<0.05$ [between lane 3 and lane 4]. (**C**) The ratio of nuclear-localized xIQGAP1-GFP in cells injected with *xDVL1*-MO, *xDVL2*-MO and *xDVL3*-MO in *Xenopus* animal cap cells at stage 10. Lane 1: n = 1424, 23.0%, lane 2: n = 1306, 21.6%, lane 3: n = 1702, 37.6%, lane 4: n = 1409, 16.6%. $P>0.1$ [between lane 1 and lane 2], $P<0.01$ [between lane 3 and lane 4]. (**D**) Cytoplasmic and nuclear distribution of xIQGAP1 in animal cap cells. MYC-tagged *xIQGAP1* mRNA (100 pg) was injected into the animal poles of 4-cell stage embryos. The following procedure is indicated in Figure 2C. $P<0.1$ [between lane 5 and lane 6], $P<0.1$ [between lane 7 and lane 8]. (**E**) Interaction between ectopically-expressed xDVL2 and xIQGAP1 in HEK 293T cells. The transfected cultured cells were stimulated with recombinant human Wnt3A for 6 hours in lanes 3 and 4. The bars represent the IP/Input ratios of xDVL2-FLAG for each transfection. Error bars represent standard deviation of the mean in three experiments. Statistical significance was determined by Student's *t*-test. $P<0.1$ [between lane 2 and lane 4].

doi:10.1371/journal.pone.0060865.g003

GFP were mainly localized in the nuclei regardless of Wnt stimulation. Moreover, *xIQGAP1-DBR* reduced expression of the Wnt target genes induced by *xDVL2*, *Xwnt-8* and *β-catenin*. Taken together, these results suggest that the domains mediating binding between xIQGAP1 and xDVL2 play important roles in both their nuclear localization and their Wnt-stimulated activities.

In vertebrates, DVL1, DVL2 and DVL3 have redundant function in part [51], [52]. Depletion of all three xDVLs; xDVL1,

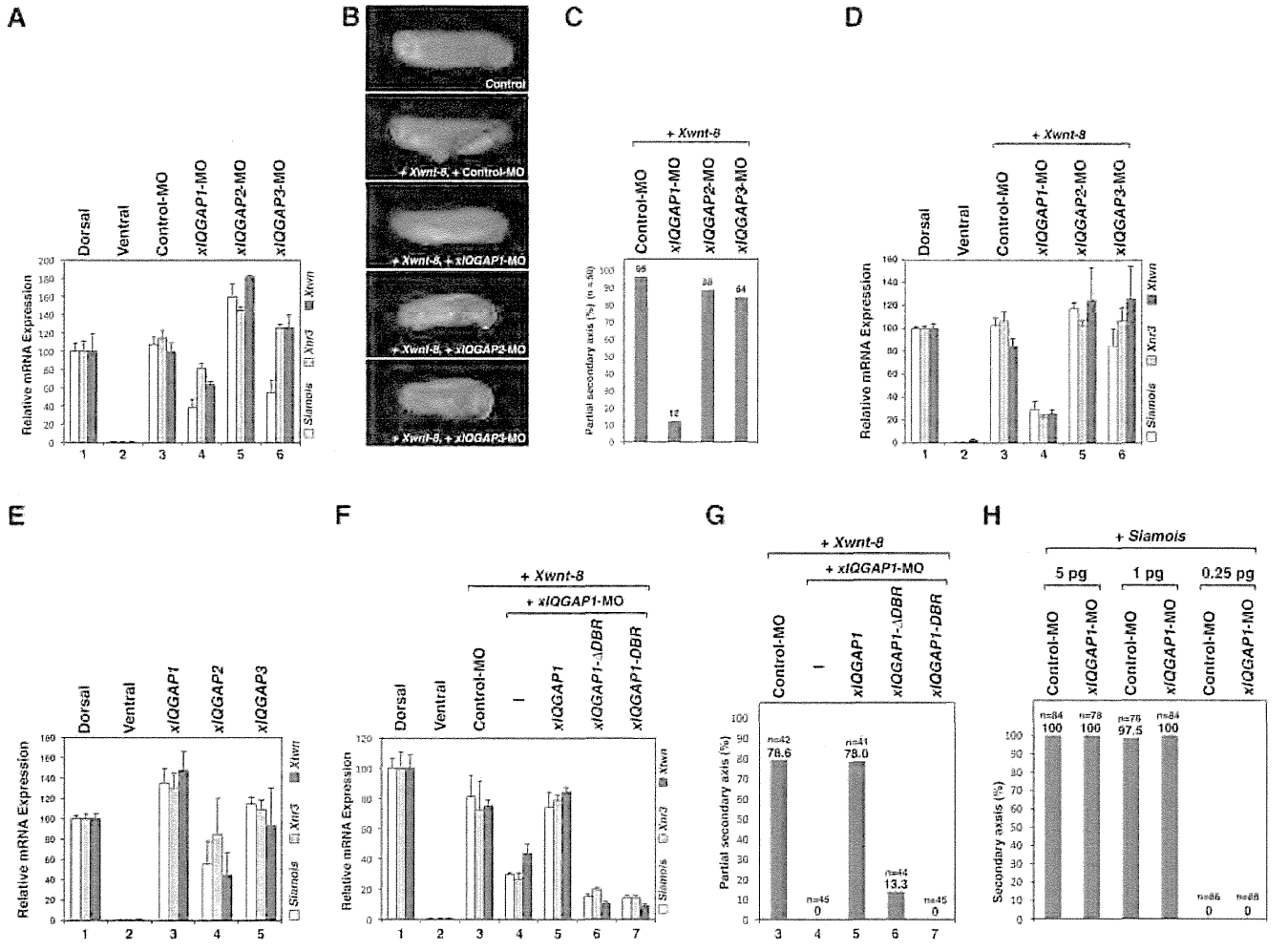

Figure 4. xIQGAP1 is required for the canonical Wnt pathway during early embryogenesis. (**A**) Quantitative RT-PCR analysis of early dorsal Wnt target genes (n = 3). Each indicated morpholino (15 ng) was injected into two dorsal blastomeres of 4-cell embryos. RNAs from dissected dorsal sectors of injected embryos were extracted at stage 10. RNAs from dissected dorsal and ventral sectors of uninjected embryos were used as controls. The value obtained for each gene was normalized to the level of ODC (ornithine decarboxylase). The value of dorsal sectors was set to 100 and other values were computed. Error bars represent standard deviation of the mean in three experiments. Statistical significance was determined by Student's *t*-test for each marker gene. The highest P values in three marker genes were chosen as a representative, as follows: $P<0.05$ [between lane 3 and lane 4], $P<0.05$ [between lane 3 and lane 5], $P>0.1$ [between lane 3 and lane 6]. (**B**) Phenotypes of injected embryos at stage 30. Control (upper panel). *Xwnt-8* mRNA (0.5 pg) was co-injected with *xIQGAP1-*, *xIQGAP2-* or *xIQGAP3*-MO (15 ng) into two ventral blastomeres of 4-cell embryos. (**C**) The ratio of injected embryos exhibiting a partial secondary axis. (**D**) Quantitative RT-PCR analysis of early dorsal Wnt target genes (n = 3). *xIQGAP1-*, *xIQGAP2-* or *xIQGAP3*-MO (15 ng) and *Xwnt-8* (0.5 pg) (20 pg) mRNA were ventrally co-injected. RNAs from dissected ventral sectors of injected embryos were extracted at stage 10. The following procedure is indicated in Figure 4A. $P<0.01$ [between lane 3 and lane 4], $P<0.1$ [between lane 3 and lane 5], $P>0.1$ [between lane 3 and lane 6]. (**E**) Quantitative RT-PCR analysis of early dorsal Wnt target genes (n = 3). *xIQGAP1*, *xIQGAP2* or *xIQGAP3* (400 pg) mRNA was dorsally injected. The following procedure is indicated in Figure 4A. $P<0.05$ [between lane 1 and lane 3], $P<0.01$ [between lane 1 and lane 4], $P>0.1$ [between lane 1 and lane 5]. (**F**) Quantitative RT-PCR analysis of early dorsal Wnt target genes (n = 3). *xIQGAP1*-MO (15 ng) and *Xwnt-8* (0.5 pg) (20 pg) mRNA were ventrally co-injected with *xIQGAP1* constructs: *xIQGAP1* (400 pg), *xIQGAP1-ΔDBR* (400 pg), *xIQGAP1-DBR* (400 pg) mRNA. RNAs from dissected ventral sectors of injected embryos were extracted at stage 10. The following procedure is indicated in Figure 4A. $P<0.05$ [between lane 3 and lane 4], $P<0.05$ [between lane 4 and lane 5], $P<0.05$ [between lane 5 and lane 6], $P<0.05$ [between lane 5 and lane 7]. (**G**) The ratio of injected embryos exhibiting a partial secondary axis. The numbered lanes indicate the injected mRNAs and MOs consistent with the numbering in Figure F. (**H**) The ratio of injected embryos that exhibited a secondary axis. Control-MO (15 ng) or *xIQGAP1*-MO (15 ng) was co-injected with *Siamois* mRNA (indicated dose).
doi:10.1371/journal.pone.0060865.g004

xDVL2 and xDVL3, did reduce severely the nuclear localization of xIQGAP1 rather than only xDVL2 depletion. Moreover, induction of Wnt target genes and formation of the secondary axis by *Xwnt-8* or *β-catenin* was suppressed by the depletion of all three xDVLs, but not by the depletion of xDVL2 alone. However, xDVL2 expression could rescue suppression of Wnt target genes by the depletion of all three xDVLs. These results suggest that xDVL1, xDVL2 and xDVL3 also function redundantly in Wnt signaling involving xIQGAP1. On the other hand, we showed that all IQGAP isoforms bound to each DVL isoform, nevertheless only IQGAP1 was necessary for Wnt signaling. Previous report also showed the functional differences, their subcellular localization and the interaction with binding proteins among IQGAP isoforms in many different cellular processes [36]. Therefore, unidentified binding molecules might cause the functional

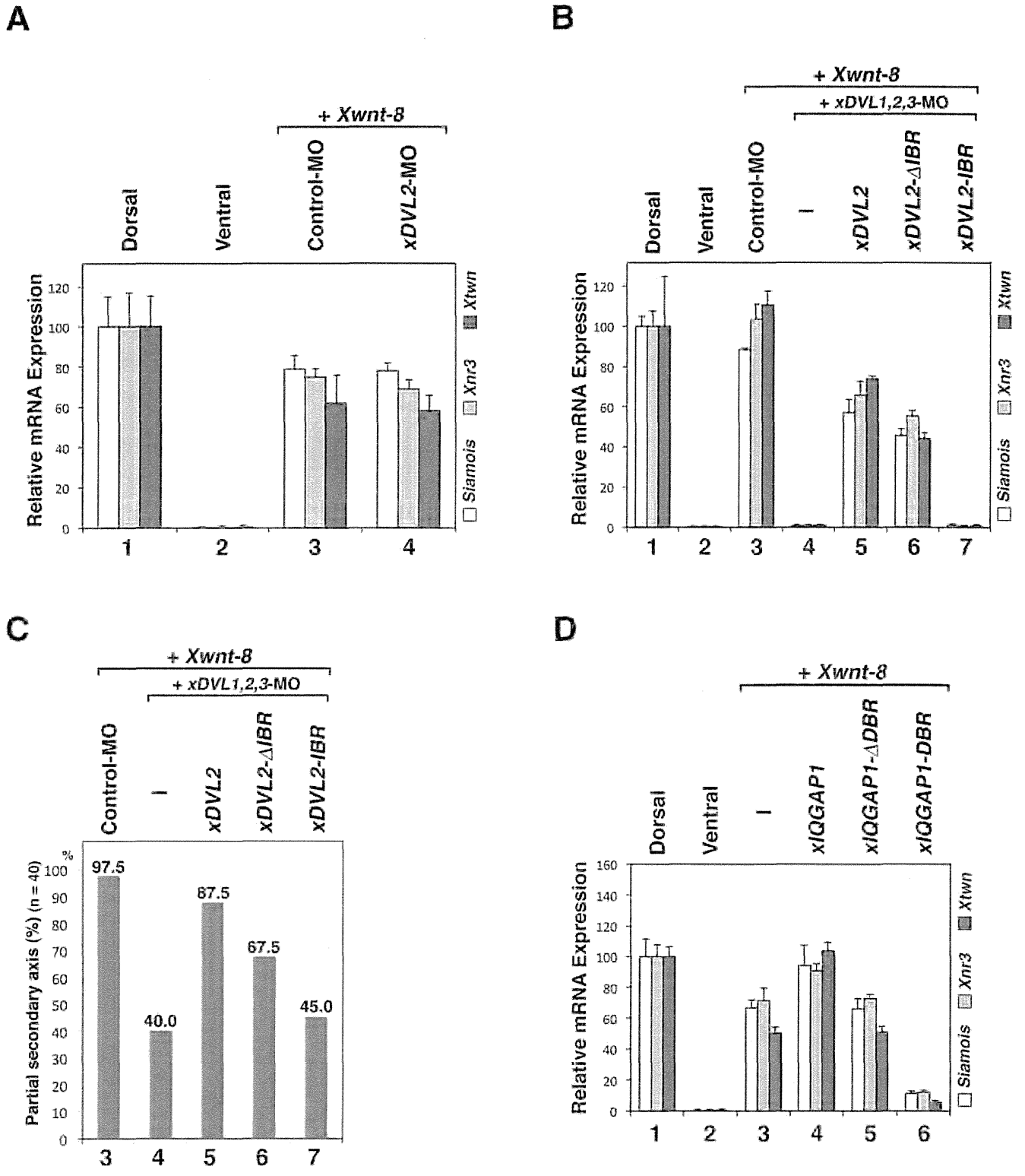

Figure 5. The role of the xIQGAP1-binding region of xDVL2 in canonical Wnt signaling during early embryogenesis. (**A**) Quantitative RT-PCR analysis of early dorsal Wnt target genes (n = 3). Control-MO (15 ng) or *xDVL2*-MO (15 ng) was ventrally co-injected with *Xwnt-8* (0.5 pg) mRNA. RNAs from dissected ventral sectors of injected embryos were extracted at stage 10. The following procedure is indicated in Figure 4A. Error bars represent standard deviation of the mean in three experiments. Statistical significance was determined by Student's *t*-test for each marker gene. The highest P values in three marker genes were chosen as a representative, as follows: $P>0.1$ [between lane 3 and lane 4]. (**B**) Quantitative RT-PCR analysis of early dorsal Wnt target genes (n = 3). *xDVL1*-MO (10 ng), *xDVL2*-MO (10 ng), *xDVL3*-MO (10 ng) and *Xwnt-8* (0.5 pg) mRNA were ventrally co-injected with *xDVL2* constructs: *xDVL2* (25 pg), *xDVL2-ΔIBR* (25 pg), *xDVL2-IBR* (25 pg) mRNA. RNAs from dissected ventral sectors of injected embryos were extracted at stage 10. The following procedure is indicated in Figure 4A. $P<0.05$ [between lane 3 and lane 4], $P<0.05$ [between lane 4 and lane 5], $P<0.1$ [between lane 5 and lane 6], $P<0.05$ [between lane 5 and lane 7]. (**C**) The ratio of injected embryos that exhibited a partial

secondary axis. The numbered lanes indicate the injected mRNAs and MOs consistent with the numbering in Figure B. (**D**) Quantitative RT-PCR analysis of early dorsal Wnt target genes (n = 3). *Xwnt-8* (0.5 pg) mRNA was ventrally co-injected with *xIQGAP1* constructs: *xIQGAP1* (400 pg), *xIQGAP1-ΔDBR* (1 ng), *xIQGAP1-DBR* (1 ng) mRNA. The following procedure is indicated in Figure 4A. P<0.01 [between lane 3 and lane 4], P>0.1 [between lane 3 and lane 5], P<0.05 [between lane 3 and lane 6].
doi:10.1371/journal.pone.0060865.g005

differences among IQGAP isoforms. Further molecular analyses will be needed to clarify the different roles of IQGAP isoforms.

Supporting Information

Figure S1 Expression of *Xenopus* DVL and IQGAP1 isoforms and confirmation of the morpholino specificity. Reverse transcription–polymerase chain reaction analysis was performed using total RNA extracted from *Xenopus* embryos at different stages of development and from different regions. *Ornithine decarboxylase* (*ODC*) was used as an internal control. (**A**) Temporal expression patterns. U, unfertilized eggs. The numbers indicate developmental stages. (**B**) Spatial expression patterns. Embryos were dissected at stage 10, and dissections were performed as shown in the right panel. D, dorsal; Vn, ventral; A, animal; M, marginal; Vg, vegetal; H, head. (**C**) Morpholino (MO) (10 ng) and FLAG-tagged mRNAs (100 pg) were co-injected with *β-globin-FLAG* mRNA (100 pg) as loading control into the animal poles of 4-cell stage embryos, and the injected animal caps were dissected at stage 10. Lysates from the animal caps were subjected to Western blotting with anti-FLAG antibody (M2, Sigma).
(TIF)

Figure S2 Localization of xDVL2 and xIQGAP1 GFP constructs in *Xenopus* animal cap cells at stage 10. (**A**) GFP signals (left panels). DAPI staining (center panels). Merge (right panels). xDVL2-*Δ*IBR-GFP (upper panels). xDVL2-IBR-GFP (second panels). xIQGAP1-*Δ*DBR-GFP (third panels). xIQGAP1-DBR-GFP (bottom panels). (**B-E**) The ratio of cells that had nuclear fluorescence signals. The average of ratio was taken with six explants in 3 independent experiments (See Materials and Methods). Error bars represent standard deviation of the mean with six explants. Statistical significance was determined by Student's *t*-test. (**B**) The ratio of nuclear-localized xDVL2-*Δ*IBR-GFP. Lane 1: n = 499, 22.4%, lane 2: n = 349, 23.8%. P>0.1 [between lane 1 and lane 2]. (**C**) The ratio of nuclear-localized xDVL2-IBR-GFP. Lane 1: n = 740, 78.9%, lane 2: n = 420, 87.6%. P>0.1 [between lane 1 and lane 2]. (**D**) The ratio of nuclear localized xIQGAP1-*Δ*DBR-GFP. Lane 1: n = 1205, 13.0%, lane 2: n = 410, 14.6%. P>0.1 [between lane 1 and lane 2]. (**e**) The ratio of nuclear localized xIQGAP1-DBR-GFP. Lane 1: n = 1598, 80.6%, lane 2: n = 408, 92.7%. P<0.01 [between lane 1 and lane 2].
(TIF)

Figure S3 Effects of over-expression of *xIQGAP1* and *xDVL2* constructs on the nuclear localization of xDVL2-GFP and xIQGAP1-GFP. The ratio of cells that had nuclear fluorescence signals. The average of ratio was taken with six explants in 3 independent experiments (See Materials and Methods). Error bars represent standard deviation of the mean with six explants. Statistical significance was determined by Student's *t*-test. (**A**) The ratio of nuclear-localized xDVL2-GFP in cells expressing various *xIQGAP1* constructs: *xIQGAP1*, *xIQGAP1-ΔDBR* or *xIQGAP1-DBR* mRNA. Lane 1: n = 1038, 22.1%, lane 2: n = 495, 31.1%, lane 3: n = 698, 26.5%, lane 4: n = 262, 55.7%, lane 5: n = 1171, 41.8%, lane 6: n = 655, 52.7%, lane 7: n = 611, 27.7%, lane 8: n = 520, 61.0%. P<0.1 [between lane 1 and lane 2], P>0.1 [between lane 1 and lane 3], P<0.01 [between lane 1 and lane 4], P<0.01 [between lane 5 and lane 6], P<0.01 [between lane 5 and lane 7], P<0.01 [between lane 5 and lane 8]. (**B**) The ratio of nuclear localized xIQGAP1-GFP in cells expressing various *xDVL2* constructs: *xDVL21*, *xDVL21-ΔIBR* or *xDVL2-IBR* mRNA. Lane 1: n = 801, 22.0%, lane 2: n = 726, 23.3%, lane 3: n = 765, 21.4%, lane 4: n = 1223, 22.2%, lane 5: n = 1171, 36.5%, lane 6: n = 362, 37.6%, lane 7: n = 641, 22.3%, lane 8: n = 549, 33.2%. P>0.1 [between lane 1 and lane 2], P>0.1 [between lane 1 and lane 3], P>0.1 [between lane 1 and lane 4], P>0.1 [between lane 5 and lane 6], P<0.01 [between lane 5 and lane 7], P>0.1 [between lane 5 and lane 8].
(TIF)

Figure S4 The effects of xIQGAP isoforms and xIQGAP1 mutated constructs. (**A, C**) Quantitative RT-PCR analysis of early dorsal Wnt target genes (n = 3). *xIQGAP1*-MO (15 ng) and *xDVL2* (50 pg) or *β-catenin* (20 pg) mRNA were ventrally co-injected with *xIQGAP1* constructs: *xIQGAP1* (400 pg), *xIQGAP1-ΔDBD* (400 pg), *xIQGAP1-DBD* (400 pg) mRNA. RNAs from dissected ventral sectors of injected embryos were extracted at stage 10. RNAs from dissected dorsal and ventral sectors of uninjected embryos were used as controls. The value obtained for each gene was normalized to the level of ODC (ornithine decarboxylase). The value of dorsal sectors was set to 100 and other values were computed. Error bars represent standard deviation of the mean in three experiments. Statistical significance was determined by Student's *t*-test for each marker gene. The highest P values in three marker genes were chosen as a representative. (**A**) P<0.05 [between lane 3 and lane 4], P<0.05 [between lane 4 and lane 5], P<0.05 [between lane 5 and lane 6], P<0.05 [between lane 5 and lane 7]. (**C**) P<0.05 [between lane 3 and lane 4], P<0.05 [between lane 4 and lane 5], P<0.05 [between lane 5 and lane 6], P<0.05 [between lane 5 and lane 7]. (**B, D**) The ratio of injected embryos exhibiting a partial secondary axis. The numbered lanes indicate the injected mRNAs and MOs consistent with the numbering in Figure **A** and **C**, respectively.
(TIF)

Figure S5 The effects of *IQGAP1* on the Wnt target genes in cultured cells. RT-PCR analysis of Wnt target genes in NIH3T3 cells. The transfected cultured cells were stimulated with the Wnt-3A conditioned medium from L-Wnt-3A cells for 24 hours. The condition medium from L cells was used for unstimulated control. GAPDH was used for normalization of cDNA samples. (**A**) siRNAs were transfected. (**B**) xIQGAP1 or xIQGAP1-DBD was transfected.
(TIF)

Figure S6 The effects of xDVL2 and xIQGAP1 mutated constructs. (**A, B**) Quantitative RT-PCR analysis of early dorsal Wnt target genes (n = 3). *xDVL2* (50 pg) or *β-catenin* (20 pg) mRNA were ventrally co-injected with *xIQGAP1* constructs: *xIQGAP1* (400 pg), *xIQGAP1-ΔDBD* (1 ng), *xIQGAP1-DBD* (1 ng) mRNA. The following procedure is indicated in Figure S4A. (**A**) P<0.1 [between lane 3 and lane 4], P<0.05 [between lane 3 and lane 5], P<0.05 [between lane 3 and lane 6]. (**B**) P<0.05 [between lane 3 and lane 4], P>0.1 [between lane 3 and lane 5], P<0.05 [between lane 3 and lane 6].
(TIF)

Acknowledgments

We thank M. Lamphier for critical reading of the manuscript.

Author Contributions

Conceived and designed the experiments: HS . Performed the experiments: TG AS MS SA KS. Analyzed the data: TG AS MS SA KS. Contributed reagents/materials/analysis tools: SI TN. Wrote the paper: HS TG.

References

1. Logan CY, Nusse R (2004) The Wnt signaling pathway in development and disease. Annu Rev Cell Dev Biol 20: 781–810.
2. Clevers H (2006) Wnt/beta-catenin signaling in development and disease. Cell 127: 469–480.
3. Peifer M, Polakis P (2000) Wnt signaling in oncogenesis and embryogenesis–a look outside the nucleus. Science 287: 1606–1609.
4. Wodarz A, Nusse R (1998) Mechanisms of Wnt signaling in development. Annu Rev Cell Dev Biol 14: 59–88.
5. Bienz M, Clevers H (2000) Linking colorectal cancer to Wnt signaling. Cell 103: 311–320.
6. Gumbiner BM (1997) Carcinogenesis: a balance between beta-catenin and APC. Curr Biol 7: R443–R446.
7. Miller JR, Moon RT (1997) Analysis of the signaling activities of localization mutants of beta-catenin during axis specification in *Xenopus*. J Cell Biol 139: 229–243.
8. Sokol S, Christian JL, Moon RT, Melton DA (1991) Injected Wnt RNA induces a complete body axis in *Xenopus* embryos. Cell 67: 741–752.
9. Funayama N, Fagotto F, McCrea P, Gumbiner BM (1995) Embryonic axis induction by the armadillo repeat domain of beta-catenin: evidence for intracellular signaling. J Cell Biol 128: 959–968.
10. Fagotto F, Funayama N, Gluck U, Gumbiner BM (1996) Binding to cadherins antagonizes the signaling activity of beta-catenin during axis formation in *Xenopus*. J Cell Biol 132: 1105–1114.
11. Sokol SY (1996) Analysis of Dishevelled signalling pathways during *Xenopus* development. Curr Biol 6: 1456–1467.
12. Carnac G, Kodjabachian L, Gurdon JB, Lemaire P (1996) The homeobox gene Siamois is a target of the Wnt dorsalisation pathway and triggers organiser activity in the absence of mesoderm. Development 122: 3055–3065.
13. Glinka A, Delius H, Blumenstock C, Niehrs C (1996) Combinatorial signalling by Xwnt-11 and Xnr3 in the organizer epithelium. Mech Dev 60: 221–231.
14. Laurent MN, Blitz IL, Hashimoto C, Rothbächer U, Cho KW (1997) The *Xenopus* homeobox gene twin mediates Wnt induction of goosecoid in establishment of Spemann's organizer. Development 124: 4905–4916.
15. Klingensmith J, Yang Y, Axelrod JD, Beier DR, Perrimon N, et al. (1996) Conservation of dishevelled structure and function between flies and mice: isolation and characterization of Dvl2. Mech Dev 58: 15–26.
16. Pizzuti A, Amati F, Calabrese G, Mari A, Colosimo A, et al. (1996) cDNA characterization and chromosomal mapping of two human homologues of the Drosophila dishevelled polarity gene. Hum Mol Genet 5: 953–358.
17. Lee YN, Gao Y, Wang HY (2008) Differential mediation of the Wnt canonical pathway by mammalian Dishevelleds-1, -2, and -3. Cell Signal 20: 443–452.
18. Capelluto DG, Kutateladze TG, Habas R, Finkielstein CV, He X, et al. (2002) The DIX domain targets dishevelled to actin stress fibres and vesicular membranes. Nature 419: 726–729.
19. Pan WJ, Pang SZ, Huang T, Guo HY, Wu D, et al. (2004) Characterization of function of three domains in dishevelled-1: DEP domain is responsible for membrane translocation of dishevelled-1. Cell Res 14: 324–330.
20. Moriguchi T, Kawachi K, Kamakura S, Masuyama N, Yamanaka H, et al. (1999) Distinct domains of mouse dishevelled are responsible for the c-Jun N-terminal kinase/stress-activated protein kinase activation and the axis formation in vertebrates. J Biol Chem 274: 30957–30962.
21. Rothbächer U, Laurent MN, Deardorff MA, Klein PS, Cho KW, et al. (2000) Dishevelled phosphorylation, subcellular localization and multimerization regulate its role in early embryogenesis. EMBO J 19: 1010–1022.
22. Axelrod JD, Miller JR, Shulman JM, Moon RT, Perrimon N (1998) Differential recruitment of Dishevelled provides signaling specificity in the planar cell polarity and Wingless signaling pathways. Genes Dev 12: 2610–2622.
23. Boutros M, Paricio N, Strutt DI, Mlodzik M (1998) Dishevelled activates JNK and discriminates between JNK pathways in planar polarity and wingless signaling. Cell 94: 109–118.
24. Gan XQ, Wang JY, Xi Y, Wu ZL, Li YP, et al. (2008) Nuclear Dvl, c-Jun, beta-catenin, and TCF form a complex leading to stabilization of beta-catenin-TCF interaction. J Cell Biol 180: 1087–1100.
25. Kuroda S, Fukata M, Kobayashi K, Nakafuku M, Nomura N, et al. (1996) Identification of IQGAP as a putative target for the small GTPases, Cdc42 and Rac1. J Biol Chem 271: 23363–23367.
26. Joyal JL, Annan RS, Ho YD, Huddleston ME, Carr SA, et al. (1997) Calmodulin modulates the interaction between IQGAP1 and Cdc42. Identification of IQGAP1 by nanoelectrospray tandem mass spectrometry. J Biol Chem 272: 15419–15425.
27. Erickson JW, Cerione RA, Hart MJ (1997) Identification of an actin cytoskeletal complex that includes IQGAP and the Cdc42 GTPase. J Biol Chem 272: 24443–24447.
28. Weissbach L, Bernards A, Herion DW (1998) Binding of myosin essential light chain to the cytoskeleton-associated protein IQGAP1. Biochem Biophys Res Commun 251: 269–276.
29. Mateer SC, McDaniel AE, Nicolas V, Habermacher GM, Lin MJ, et al. (2002) The mechanism for regulation of the F-actin binding activity of IQGAP1 by calcium/calmodulin. J Biol Chem 277: 12324–12333.
30. Li Z, Sacks DB (2003) Elucidation of the interaction of calmodulin with the IQ motifs of IQGAP1. J Biol Chem 278: 4347–4352.
31. Roy M, Li Z, Sacks DB (2004) IQGAP1 binds ERK2 and modulates its activity. J Biol Chem 279: 17329–17337.
32. Li Q, Stuenkel EL (2004) Calcium negatively modulates calmodulin interaction with IQGAP1. Biochem Biophys Res Commun 317: 787–795.
33. Kuroda S, Fukata M, Nakagawa M, Fujii K, Nakamura T, et al. (1998) Role of IQGAP1, a target of the small GTPases Cdc42 and Rac1, in regulation of E-cadherin- mediated cell-cell adhesion. Science 281: 832–835.
34. Briggs MW, Li Z, Sacks DB (2002) IQGAP1-mediated stimulation of transcriptional co-activation by beta-catenin is modulated by calmodulin. J Biol Chem 277: 7453–7465.
35. Brown MD, Sacks DB (2006) IQGAP1 in cellular signaling: bridging the GAP. Trends Cell Biol 16: 242–249.
36. White CD, Brown MD, Sacks DB (2009) IQGAPs in cancer: a family of scaffold proteins underlying tumorigenesis. FEBS Lett 583: 1817–1824.
37. Schmidt VA, Chiariello CS, Capilla E, Miller F, Bahou WF (2008) Development of hepatocellular carcinoma in Iqgap2-deficient mice is IQGAP1 dependent. Mol Cell Biol 28: 1489–1502.
38. Yamashiro S, Noguchi T, Mabuchi I (2003) Localization of two IQGAPs in cultured cells and early embryos of *Xenopus laevis*. Cell Motil Cytoskeleton 55: 36–50.
39. Yamashiro S, Abe H, Mabuchi I (2007) IQGAP2 is required for the cadherin-mediated cell-to-cell adhesion in *Xenopus laevis* embryos. Dev Biol 308: 485–493.
40. Itoh K, Brott BK, Bae GU, Ratcliffe MJ, Sokol SY (2005) Nuclear localization is required for Dishevelled function in Wnt/beta-catenin signaling. J Biol 4: 3.
41. Shimizu K, Gurdons JB (1999) A quantitative analysis of signal transduction from activin receptor to nucleus and its relevance to morphogen gradient interpretation. Proc Natl Acad Sci U S A 96: 6791–6796.
42. Ohnishi E, Goto T, Sato A, Kim MS, Iemura S, et al. (2010) Nemo-like kinase, an essential effector of anterior formation, functions downstream of p38 mitogen-activated protein kinase. Mol Cell Biol 30: 675–683.
43. Sato A, Shibuya H (2013) WNK Signaling Is Involved in Neural Development via Lhx8/Awh Expression. PLoS One 8: e55301.
44. Natsume T, Yamauchi Y, Nakayama H, Shinkawa T, Yanagida M, et al. (2002) A direct nanoflow liquid chromatography-tandem mass spectrometry system for interaction proteomics. Anal Chem 74: 4725–4733.
45. Bryja V, Schulte G, Arenas E (2007) Wnt-3a utilizes a novel low dose and rapid pathway that does not require casein kinase 1-mediated phosphorylation of Dvl to activate beta-catenin. Cell Signal 19: 610–616.
46. Song DH, Sussman DJ, Seldin DC (2000) Endogenous protein kinase CK2 participates in Wnt signaling in mammary epithelial cells. J Biol Chem 275: 23790–23797.
47. Bastock R, Strutt H, Strutt D (2003) Strabismus is asymmetrically localised and binds to Prickle and Dishevelled during Drosophila planar polarity patterning. Development 130: 3007–3014.
48. Sun TQ, Lu B, Feng JJ, Reinhard C, Jan YN, et al. (2001) PAR-1 is a Dishevelled-associated kinase and a positive regulator of Wnt signalling. Nat Cell Biol 3: 628–636.
49. Schwarz-Romond T, Metcalfe C, Bienz M (2007) Dynamic recruitment of axin by Dishevelled protein assemblies. J Cell Sci 120: 2402–2412.
50. Strovel ET, Wu D, Sussman DJ (2000) Protein phosphatase 2Calpha dephosphorylates axin and activates LEF-1-dependent transcription. J Biol Chem 275: 2399–2403.
51. Hamblet NS, Lijam N, Ruiz-Lozano P, Wang J, Yang Y, et al. (2002) Dishevelled 2 is essential for cardiac outflow tract development, somite segmentation and neural tube closure. Development 129: 5827–5838.
52. Etheridge SL, Ray S, Li S, Hamblet NS, Lijam N, et al. (2008) Dishevelled 3 Functions in Redundant Pathways with Dishevelled 1 and 2 in Normal Cardiac Outflow Tract, Cochlea, and Neural Tube Development. PLoS Genet 4: e1000259.

Molecular Cell
Article

Long Noncoding RNA NEAT1-Dependent SFPQ Relocation from Promoter Region to Paraspeckle Mediates IL8 Expression upon Immune Stimuli

Katsutoshi Imamura,[1] Naoto Imamachi,[2] Gen Akizuki,[2] Michiko Kumakura,[3] Atsushi Kawaguchi,[3] Kyosuke Nagata,[3] Akihisa Kato,[4] Yasushi Kawaguchi,[4] Hiroki Sato,[5] Misako Yoneda,[5] Chieko Kai,[5] Tetsushi Yada,[6] Yutaka Suzuki,[7] Toshimichi Yamada,[8] Takeaki Ozawa,[8] Kiyomi Kaneki,[9] Tsuyoshi Inoue,[9] Mika Kobayashi,[9] Tatsuhiko Kodama,[9] Youichiro Wada,[2,9] Kazuhisa Sekimizu,[1] and Nobuyoshi Akimitsu[2,*]

[1]Graduate School of Pharmaceutical Sciences, The University of Tokyo, Tokyo 113-0033, Japan
[2]Radioisotope Centre, The University of Tokyo, Tokyo 113-0032, Japan
[3]Department of Infection Biology, Faculty of Medicine & Graduate School of Comprehensive Human Sciences, University of Tsukuba, Tsukuba 305-8575, Japan
[4]Division of Molecular Virology, Department of Microbiology and Immunology, The Institute of Medical Science, The University of Tokyo, Tokyo 108-8639, Japan
[5]Laboratory Animal Research Center, The Institute of Medical Science, The University of Tokyo, Tokyo 108-8639, Japan
[6]Department of Bioscience and Bioinformatics, Kyushu Institute of Technology Fukuoka 820-8502, Japan
[7]Department of Computational Biology, Graduate School of Frontier Sciences, The University of Tokyo, Chiba 277-8562, Japan
[8]Department of Chemistry, School of Science, The University of Tokyo, Tokyo 113-0033, Japan
[9]Laboratory for Systems Biology and Medicine, Research Centre for Advanced Science and Technology, The University of Tokyo, Tokyo 153-8904, Japan
*Correspondence: akimitsu@ric.u-tokyo.ac.jp
http://dx.doi.org/10.1016/j.molcel.2014.01.009

SUMMARY

Although thousands of long noncoding RNAs (lncRNAs) are localized in the nucleus, only a few dozen have been functionally characterized. Here we show that nuclear enriched abundant transcript 1 (NEAT1), an essential lncRNA for the formation of nuclear body paraspeckles, is induced by influenza virus and herpes simplex virus infection as well as by Toll-like receptor3-p38 pathway-triggered poly I:C stimulation, resulting in excess formation of paraspeckles. We found that NEAT1 facilitates the expression of antiviral genes including cytokines such as interleukin-8 (IL8). We found that splicing factor proline/glutamine-rich (SFPQ), a NEAT1-binding paraspeckle protein, is a repressor of *IL8* transcription, and that NEAT1 induction relocates SFPQ from the *IL8* promoter to the paraspeckles, leading to transcriptional activation of *IL8*. Together, our data show that NEAT1 plays an important role in the innate immune response through the transcriptional regulation of antiviral genes by the stimulus-responsive cooperative action of NEAT1 and SFPQ.

INTRODUCTION

Whole-transcriptome analyses have revealed that a new class of non-protein-coding transcripts, designated as long noncoding RNAs (lncRNAs), is transcribed from a large proportion of the mammalian genome (Carninci et al., 2005; Guttman et al., 2009; Kapranov et al., 2007). There is increasing evidence of lncRNA involvement in diverse biological processes (Chen and Carmichael, 2010; Gupta et al., 2010; Ponting et al., 2009; Yoon et al., 2013). Moreover, a large number of lncRNAs is induced by extracellular stimuli, suggesting that lncRNAs participate in stress responses (Mizutani et al., 2012; Tani et al., 2012). In addition, because lncRNAs are also implicated in many human diseases (Huarte and Rinn, 2010; Wang and Chang, 2011), understanding the precise molecular mechanisms by which lncRNAs function could prove important for developing new strategies for early diagnosis and molecular therapy. In particular, there are several emerging hypotheses on lncRNA involvement in infectious diseases (Scaria and Pasha, 2012). However, a mechanistic understanding of the role of lncRNAs in infection is limited. Hence, the functions of lncRNAs in host antiviral response have remained unclear.

The mammalian nucleus is highly organized and contains distinct structural components comprising approximately ten types of nuclear bodies, including speckles and paraspeckles, which are thought to be involved in gene regulation (Mao et al., 2011). Some of these nuclear bodies contain specific lncRNAs that regulate nuclear body function (Kapranov et al., 2007; Prasanth and Spector, 2007). Recent reports have suggested that crosstalk between architectural features of nuclear bodies and lncRNAs contributes to the precise control of gene expression. For example, speckles contain the metastasis-associated lung adenocarcinoma transcript 1 (MALAT1), a lncRNA involved in regulating the expression of several specific genes (Bernard et al., 2010; Miyagawa et al., 2012; Tano et al., 2010; Yang et al., 2011). Paraspeckles contain another lncRNA, NEAT1, which is an essential architectural component of paraspeckle

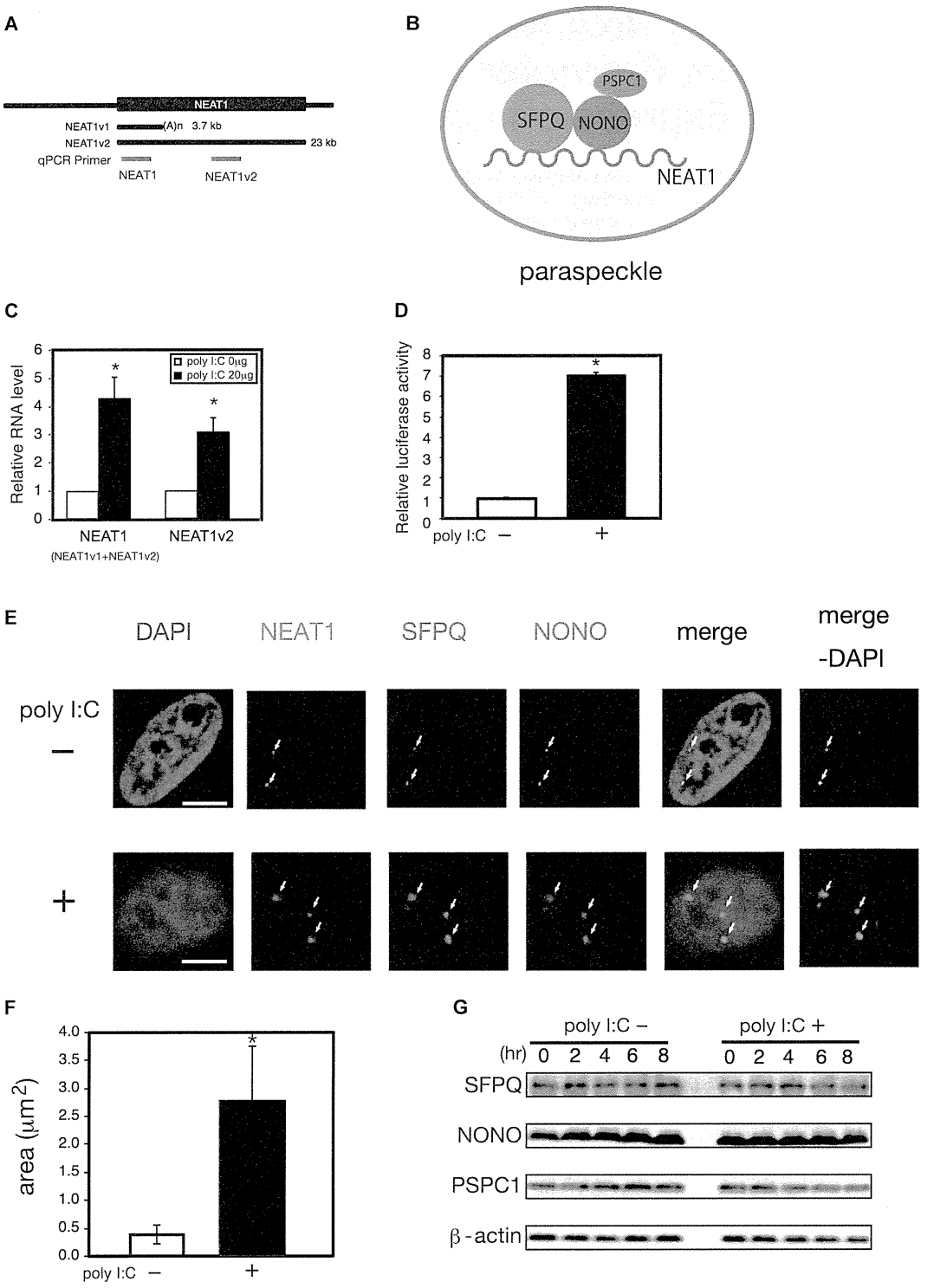

Figure 1. NEAT1 Induction and Excessive Formation of Paraspeckles by Poly I:C

(A) NEAT1 isoforms are shown schematically. The fragment positions amplified by the RT-qPCR primers are shown below.

(B) Entities of paraspeckles are shown schematically.

(legend continued on next page)

structure (Chen and Carmichael, 2009; Clemson et al., 2009; Sasaki et al., 2009; Sunwoo et al., 2009). The *NEAT1* gene (Figure 1A) produces two isoforms, 3.7 kb NEAT1v1 and 23 kb NEAT1v2 (Hutchinson et al., 2007). The effect of NEAT1v2 on the formation of paraspeckles is stronger than that of NEAT1v1 (Naganuma et al., 2012; Sasaki et al., 2009). Paraspeckles have been proposed to control several biological processes, including stress response and cellular differentiation, through control of the nuclear retention of mRNAs containing inverted repeats that form double-stranded RNA regions subject to adenosine-to-inosine editing (Fox and Lamond, 2010; Nakagawa and Hirose, 2012). Paraspeckles contain several protein factors: NONO/p54nrb, SFPQ/PSF, PSPC1, RBM14, and CPSF6 (Fox and Lamond, 2010). Among these, SFPQ and NONO form the heterodimer (Peng et al., 2002), which binds directly to NEAT1 (Sasaki et al., 2009) (Figure 1B). Several studies have demonstrated that SFPQ represses the transcription of several genes through direct promoter binding (Iacobazzi et al., 2005; Song et al., 2004; Urban et al., 2000). Recently, 35 proteins were added into the list of paraspeckle proteins (Naganuma and Hirose, 2013). Several of paraspeckle proteins are likely to be the factors involved in transcriptional control, suggesting that paraspeckles may integrate tightly coupled transcription and posttranscriptional events.

The innate immune response is crucial in the host cellular response to viral infection. Several pathogen-associated molecular pattern recognition receptors, such as the Toll-like receptors, sense the presence of viral molecules and trigger a robust program of gene expression involving the production of antiviral inflammatory cytokines, chemokines, and interferons through numerous transcriptional and posttranscriptional strategies (Arpaia and Barton, 2011; Rathinam and Fitzgerald, 2011; Thompson et al., 2011). For example, poly I:C, a double-stranded RNA (dsRNA)-mimicking immunostimulant that simulates viral infections, activates the TLR3-mediated signaling pathway, and consequently induces a set of antiviral genes (Kawai and Akira, 2010). To achieve the proper immune response, the transcriptional induction of immune response genes is highly coordinated by activators and repressors. For instance, the interleukin-8 (*IL8*) promoter is repressed by the binding of three factors in unstimulated cells (Hoffmann et al., 2002): NF-κB-repressing factor (NRF), octamer-1 (OCT-1), and deacetylation of histone proteins by histone deacetylase-1. When the cells are stimulated, NF-κB and C/EBP bind to the *IL8* promoter; C/EBP displaces OCT-1, whereas NRF switches its function to act as a coactivator. Recruitment of CREB-binding protein/p300 hyperacetylates the histones and remodels the chromatin, resulting in transcriptional activation of *IL8* gene. Although nuclear lncRNAs represent a large class of transcriptional units, the interplay between transcription factors and nuclear lncRNA to control gene expression during immune response remains to be elucidated.

RESULTS

Poly I:C Induces NEAT1 and Large Paraspeckle Formation

A previous study showed that NEAT1 is an inducible lncRNA in mice brains infected with Japanese encephalitis or rabies viruses, although it is unclear whether NEAT1 induction is a consequence of direct effect of viral infection to neural cells (Saha et al., 2006). This observation provided the rationale for the current study, which examined the relevance of NEAT1 in cellular response to viral infection. We therefore initially examined the expression levels of NEAT1 in response to transfection with poly I:C, a double-stranded RNA (dsRNA). As shown in Figure 1A, one primer set recognizes both NEAT1v1 and NEAT1v2 (total NEAT1), while the other recognizes only NEAT1v2. Expression levels of total NEAT1 and NEAT1v2 in HeLa cells and A549 cells were increased by poly I:C, but not by poly I or poly C alone (Figure 1C and Figures S1A–S1C). Treatment of the cells with either IFN-α or IFN-β induced 2′5′-OAS, an interferon response gene, but not NEAT1v2 (Figure S1D), ruling out the possibility of an indirect effect by which IFNs induced by poly I:C lead the expression of NEAT1. To examine whether upregulation of NEAT1 RNA levels by poly I:C stimulation was controlled by transcriptional regulation, we analyzed luciferase reporter activity in HeLa TO cells transfected with a luciferase reporter gene linked to a *NEAT1* promoter and found that poly I:C treatment enhanced the luciferase reporter activity (Figure 1D and Figure S1E). Next, we investigated the signaling pathway that activates transcription of the *NEAT1* gene by poly I:C stimulation. Because TLR3 is known as an intracellular sensor for dsRNAs such as poly I:C (Kawai and Akira, 2010), we tested the involvement of TLR3 in the poly I:C-induced transcriptional activation of the *NEAT1* gene. Knockdown of TLR3 reduced the levels of poly I:C-mediated NEAT1 induction compared with control cells (Figure S1H). We further examined other dsRNA sensors. We found that depletion of MDA-5, but not RIG-I, affected poly I:C-induced NEAT1 expression (Figures S1I and S1J). The effect of MDA-5 depletion for the reduction in poly I:C-induced NEAT1 expression was weaker than that for the reduction in TLR3, suggesting that TLR3 is the major receptor for inducing NEAT1 in response to poly I:C. TLR3-mediated signaling is branched to either the

(C) Total NEAT1 and NEAT1v2 levels of HeLa TO cells with or without poly I:C stimulation were quantified by RT-qPCR. The GAPDH mRNA level was used as the normalizing control. Values represent the mean ± SD (*p < 0.01, Student's t test).
(D) The luciferase reporter activity of HeLa TO cells transfected with a luciferase reporter gene harboring the *NEAT1* promoter was measured in the presence or absence of poly I:C. The activity of cotransfected pCMV-RL (Promega) was used as normalizing control. Values represent the mean ± SD (*p < 0.01, Student's t test).
(E) HeLa TO cells were transfected with and without poly I:C, followed by FISH staining and immunostaining. NEAT1 (green), SFPQ (magenta), NONO (red), and nuclei stained with DAPI (blue) are shown.
(F) The mean size of NEAT1 control cell foci (white bar; n = 50) and that of cells transfected with poly I:C (black bar; n = 50) was determined by FISH. Values represent the mean ± SD (*p < 0.01, Student's t test).
(G) The protein levels of paraspeckle proteins SFPQ, NONO, and PSPC1 were analyzed by western blotting at the indicated time points posttransfection with poly I:C. β-actin was used as the loading control.

p38 or JNK pathways (Arpaia and Barton, 2011). Pretreatment with ML3403, a p38 inhibitor, but not SP600125, a JNK inhibitor, abolished poly I:C-induced NEAT1 induction (Figure S1K). As expected, poly I:C-induced phosphorylation of p38 and JNK was eliminated by ML3403 and SP600125, respectively (Figures S1L and S1M). In contrast, NF-κB was not required for poly I:C-induced NEAT1 induction (Figures S1N and S1O). These results suggest that poly I:C leads to the transcriptional activation of the *NEAT1* gene mainly through the TLR3-p38 pathway.

Previous reports have shown that NEAT1 is an essential core component for the formation of paraspeckles (Chen and Carmichael, 2009; Clemson et al., 2009; Sasaki et al., 2009; Sunwoo et al., 2009). Corresponding with previous observation, paraspeckle proteins were dispersed to the nucleoplasm in the absence of NEAT1 (Figure S1Q). Because overexpression of NEAT1 results in the excess formation of paraspeckles (Clemson et al., 2009), we hypothesized that poly I:C stimulation induces this process. Combination staining of NEAT1 and of paraspeckle proteins SFPQ, NONO, and PSPC1 showed that poly I:C treatment resulted in excess paraspeckle formation in HeLa cells (Figures 1E and 1F and Figure S1P). Western blot analysis revealed that expression levels of paraspeckle proteins SFPQ and NONO remained unaltered throughout poly I:C stimulation (Figure 1G). In the absence of NEAT1, poly I:C stimulation did not induce the formation of paraspeckles (Figure S1Q). Fluorescence recovery after photobleaching (FRAP) analysis showed that the kinetics of paraspeckle-associated SFPQ in poly I:C-stimulated cells ($t_{1/2}$ = 7.08 s) was similar to that in naive cells ($t_{1/2}$ = 6.75 s) (Figures S1R and S1S; Movies S1 and S2), suggesting that the molecular quality of SFPQ was not changed by poly I:C stimulation. These findings suggest that poly I:C stimulation relocates paraspeckle proteins from the nucleoplasm to NEAT1, consequently inducing the excess formation of paraspeckles.

Identification of NEAT1-Regulated Antiviral Genes

We investigated whether NEAT1 induction followed by excess formation of paraspeckles was involved in poly I:C-inducible gene expression (Figures 2A and 2B). Microarray analysis revealed 1,232 poly I:C-inducible genes in HeLa TO cells. The induction of 259 of these poly I:C-inducible genes was abolished by NEAT1 knockdown (Figure 2B). We also identified 113 genes that were upregulated by solo overexpression of mNeat1v2 (Figure 2B). To eliminate false positives, we selected the 85 genes that form the overlap between these two groups of genes (Figure 2B). Interestingly, many antiviral factors, such as IL8 and CCL5, and virus sensors, such as RIG-I and MDA5, were identified in this group of 85 NEAT1-regulated genes, suggesting that NEAT1 is involved in the regulation of antiviral gene expression response. A gene ontology analysis using these data supported this idea (Tables S1 and S2). RT-qPCR experiments confirmed the NEAT1-dependent expression of genes involved in antiviral function, such as *IL8* and *CCL5* (Figure 2C and Table S3). To clarify whether NEAT1v2 is necessary for IL8 mRNA induction and excess paraspeckle formation, we specifically silenced NEAT1v2 using specific siRNAs (Figures S2A, S2B, and S2E) and found that NEAT1v2 depletion eliminated the induction of IL8 mRNA and excess formation of paraspeckles in response to poly I:C treatment (Figures S2C and S2D). mNeat1v2 is more active than mNeat1v1 in the formation of paraspeckles (Figure S2F). Corresponding to these findings, the effect of mNeat1v2 on gene induction was greater than that of mNeat1v1 (Figure 2E). The induction of IL8 mRNA and the size of the paraspeckles were correlated with the levels of mNeat1v2 overexpression (Figures S2G–S2I). Interestingly, NEAT1 knockdown affected the time point at which peak levels of IL8 mRNA induction were observed following poly I:C treatment (Figure 2D; 5 hr poststimulation in control cells; 3 hr poststimulation in NEAT1 knockdown cells), suggesting that NEAT1 also affects the kinetics of IL8 mRNA induction. The expression of IFN-β, a non-NEAT1-regulated gene, was not affected by the expression level of NEAT1 (Figures 2C and 2E).

Cooperative Action of NEAT1 and SFPQ Regulates *IL8* Transcription

Since paraspeckles contain many transcriptional regulators, such as SFPQ and NONO, it is reasonable to assume that excess formation of paraspeckles would affect the expression of a subset of genes. From this viewpoint, we assumed that certain paraspeckle proteins should regulate the expression of NEAT1-regulated genes such as *IL8*. As expected, we found that the expression of IL8, but not IFN-β, was increased in both SFPQ and NONO knockdown cells, but not in PSPC1 knockdown cells (Figure 3A and Figures S3A and S3L). Both SFPQ and NONO knockdown increased the promoter activity of the *IL8* gene, but not that of the *IFNB1* gene (Figure 3B and Figure S3B). In contrast, promoter activities of the *IL8* and *IFNB1* genes were unchanged in PSPC1-depleted cells (Figure 3B). Bioinformatics analysis revealed that the SFPQ-binding motif is located just 3′ downstream of the TATA box of the human *IL8* promoter and is evolutionarily conserved in the corresponding position of primate *IL8* genes (Figure 3C, Figures S3C–S3E, and Table S3). These findings suggest that SFPQ represses the *IL8* promoter. Notably, the SFPQ-binding motif was predicted with statistical significance in the promoter region of the majority of NEAT1-regulated genes (p value: 0.0015) (Table S3). We then employed a chromatin immunoprecipitation (ChIP) experiment to examine whether SFPQ binds the *IL8* promoter in vivo and is released upon poly I:C stimulation. ChIP experiment showed that SFPQ bound the SFPQ-binding motif of *IL8* gene in naive cells (Figure 3D). Conversely, SFPQ did not bind the SFPQ-binding motif when stimulated by poly I:C (Figure 3D). We also showed that binding of SFPQ to this motif decreased in cells transfected with mNeat1v2 expression plasmid (Figure 3E). We detected concomitantly increased binding of NEAT1v2 to SFPQ in response to poly I:C (Figure 3F). Consistent with this observation, the concentrations of SFPQ and NONO within enlarged paraspeckles were increased upon poly I:C treatment (Figures S3F and S3G). We performed kinetic and dose-response analyses of SFPQ binding to NEAT1v2 after poly I:C exposure. The data showed correlations among poly I:C stimulation, SFPQ binding to NEAT1v2, and IL8 mRNA induction (Figures S3H and S3I). These results suggest that SFPQ binds the SFPQ-binding motif of the *IL8* gene, thereby repressing *IL8* transcription in naive cells, and that poly I:C treatment relocates SFPQ from the *IL8* gene to NEAT1, resulting in the formation of excess paraspeckles, which in turn leads to the transcriptional

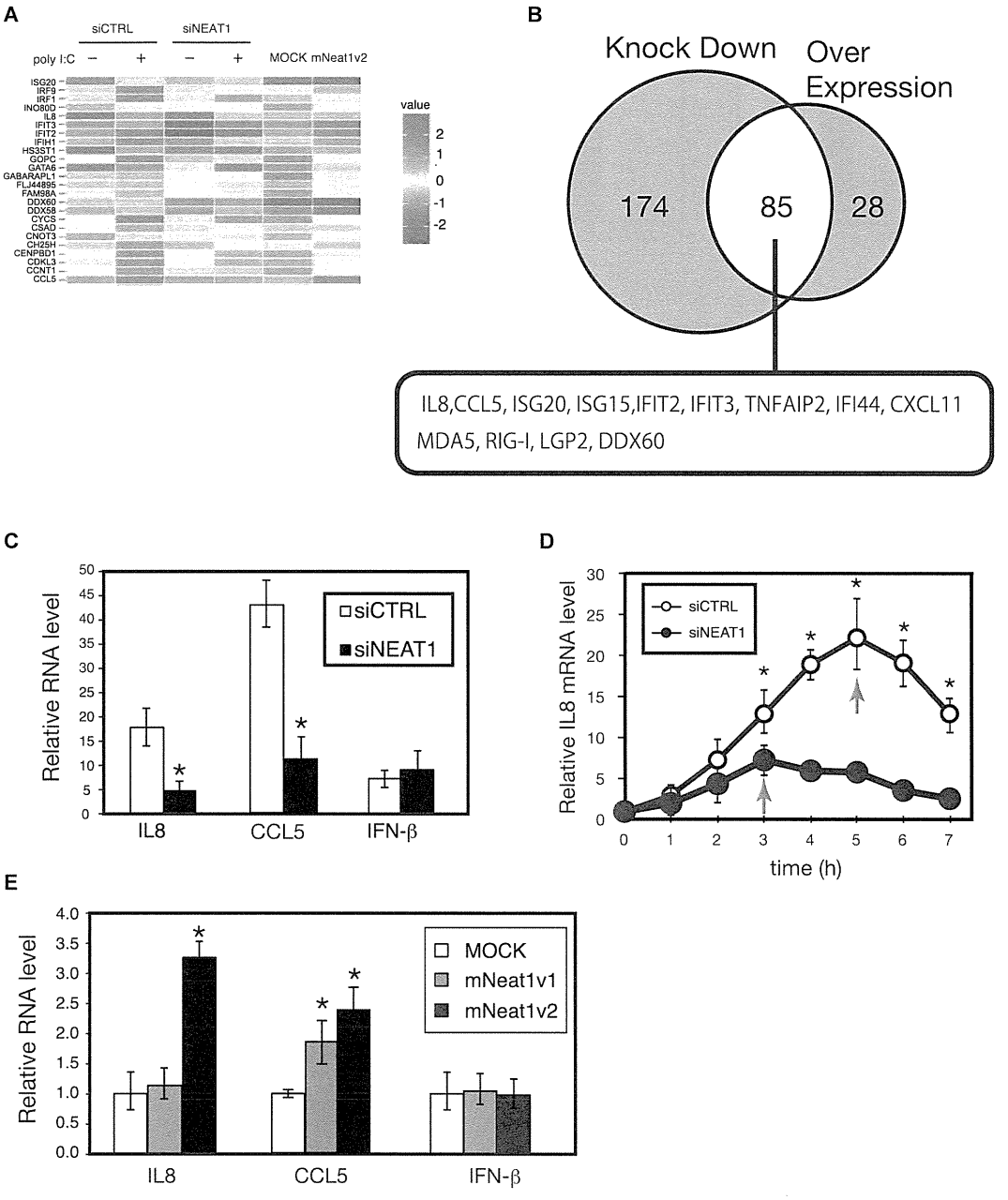

Figure 2. NEAT1-Regulated Genes

(A) Heat map image of microarray analysis of gene expression in the control cells with and without poly I:C stimulation, NEAT1 knockdown cells with and without poly I:C stimulation, and cells transfected with mock plasmid or mNeat1v2 expression plasmid alone.

(B) Venn diagram of genes with altered gene expression as identified by microarray analysis. Left circle contains the 259 poly I:C-induced genes whose induction was abolished by NEAT1 knockdown. Right circle contains the 113 genes induced by solo overexpression of mNeat1v2. Representative genes found in the overlap between these two groups are shown below.

(C) The relative mRNA levels of IL8, CCL5, and IFN-β in the poly I:C-treated cells and the nontreated cells as determined by RT-qPCR analysis. Values represent the mean ± SD (*$p < 0.01$, Student's t test).

(D) Induction kinetics of IL8 mRNA in control cells or NEAT1 knockdown cells after poly I:C stimulation.

(E) Relative mRNA levels of IL8, CCL5, and IFN-β in cells transfected with pCMV-mNeat1v1 or pCMV-mNeat1v2 compared with cells that have undergone mock transfection, as determined by RT-qPCR analysis. Values represent the mean ± SD (*$p < 0.01$, Student's t test).

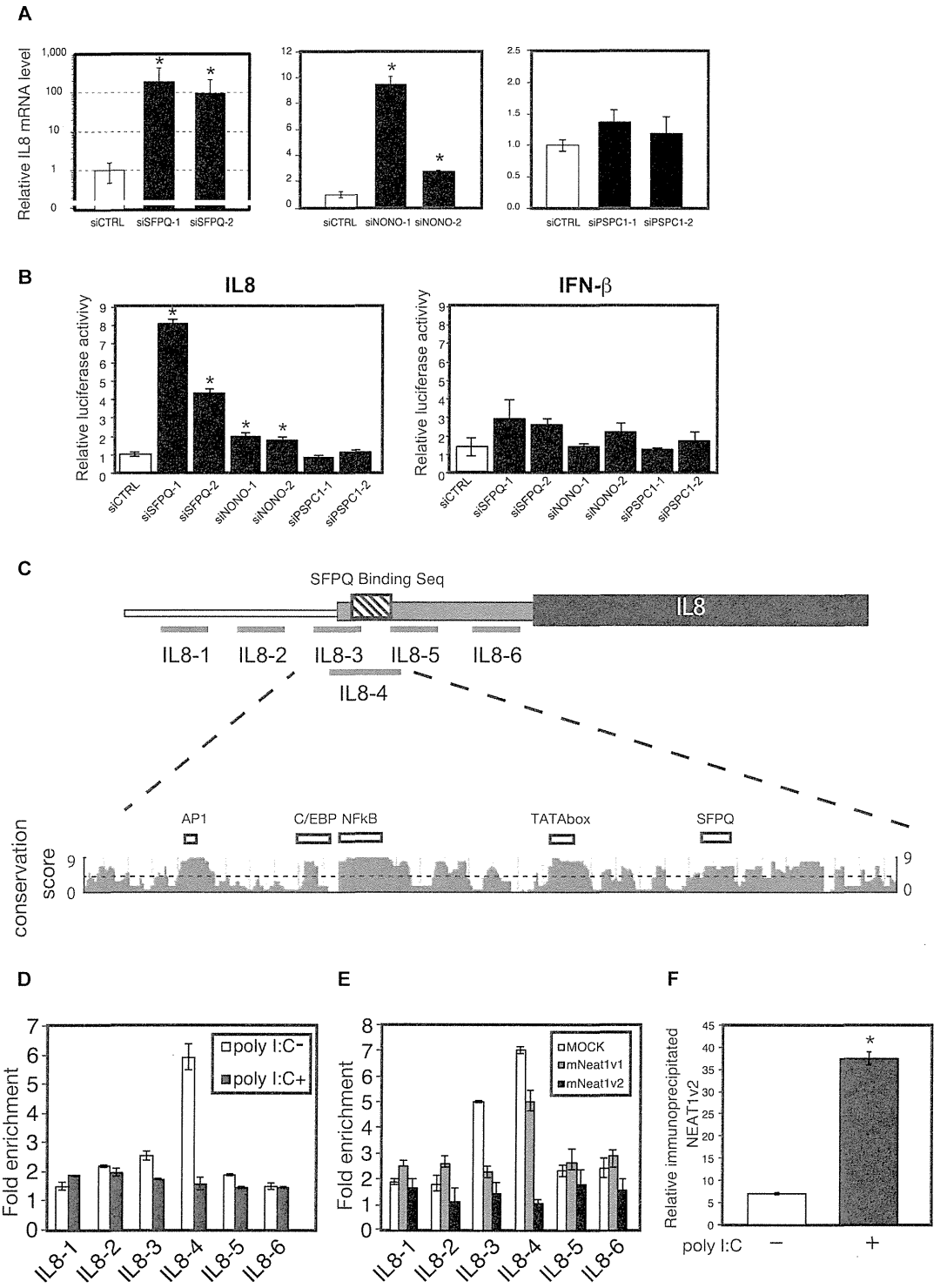

Figure 3. SFPQ-Mediated Transcriptional Repression of the *IL8* Gene and NEAT1-Mediated SFPQ Relocation

(A) IL8 mRNA levels of HeLa TO cells treated with various siRNAs as indicated. Values represent the mean ± SD (*p < 0.01, Student's t test).

(B) Luciferase reporter activities driven by the *IL8* promoter or the *INFB1* promoter were determined in cells transfected with the indicated siRNAs. Values represent the mean ± SD (*p < 0.01, Student's t test).

(legend continued on next page)

activation of *IL8*. In addition to IL8, we showed that SFPQ bound to gene promoters containing the predicted SFPQ binding motif and that SFPQ binding was reduced by poly I:C stimulation (Table S3). Next, we examined whether NEAT1 is an upstream negative regulator of SFPQ in the repression of the *IL8* gene expression. IL8 mRNA induction by SFPQ depletion was not cancelled by NEAT1 depletion (see poly I:C− condition in Figure S3J). We then examined whether the NEAT1 silencing-mediated re-repression of the IL8 gene would be cancelled by SFPQ depletion. The results showed that poly I:C-induced IL8 mRNA induction was abrogated by NEAT1 knockdown and that the NEAT1 silencing-dependent rerepression of *IL8* gene induction was cancelled by SFPQ knockdown (Figure S3J). These data support the idea in which NEAT1 plays a role as an upstream negative regulator of SFPQ in the repression of the *IL8* gene expression.

To further test our model, we generated SFPQ mutants (ΔRRM1 and ΔRRM2) that retained their ability to bind to the IL8 promoter, but were unable to bind to NEAT1v2 (Figures 4A–4C). These mutants were able to suppress the IL8 expression in response to elevated levels of mNeat1v2 (Figure 4D). Moreover, the repression activity of the mutant SFPQs was stronger than that of wild-type SFPQ (Figure 4D). Experiments using systematically constructed plasmids expressing parts of NEAT1 indicated that an approximately 15 kb portion of NEAT1 was required for IL8 mRNA induction (Figure 4E). Simultaneously, RNA immunoprecipitation (RIP) results in capturing endogenous SFPQ showed that the 15 kb portion of NEAT1 bound to SFPQ in vivo.

Since SFPQ forms a heterodimer with NONO, we examined the contribution of NONO to the function of SFPQ binding to the IL8 promoter. We found that NONO depletion reduced the binding of SFPQ to the IL8 promoter region (Figure S3K). NONO depletion did not affect the expression level of SFPQ (Figure S3L), thereby ruling out the possibility that the reduced SFPQ binding to the IL8 promoter was caused by a reduced amount of SFPQ in response to NONO depletion. These results suggest that NONO affects the binding activity of SFPQ to the IL8 promoter region. In vitro binding assays showed that SFPQ/NONO had a specific binding affinity for an IL8 promoter DNA containing the SFPQ binding motif (Figure S3M). In addition, total RNA isolated from control cells expressing excess amount of NEAT1v2 abrogated SFPQ/NONO-IL8 promoter complex, but that from control cells expressing normal amount of NEAT1 did not (Figure S3N). The destruction of SFPQ/NONO-IL8 promoter complex by total RNA isolated from the cells depleted in NEAT1 was weaker than that by total RNA from the control cells (Figure S3N).

Involvement of NEAT1 in Immune Response upon Viral Infection

We next infected culture cells with either influenza virus, herpes simplex virus 1 (HSV-1), or measles virus (MV) to examine the biological significance of our earlier observations. Influenza virus is recognized by TLR3 in host cells, leading to an immune response that includes *IL8* induction (Guillot et al., 2005). Viral-derived dsRNA produced during the HSV-1 replication cycle also triggers an immune response through TLR3 stimulation (Lafaille et al., 2012; Zhang et al., 2007). Conversely, MV infection is not sensed by TLR3 (Berghäll et al., 2006). As expected, influenza virus and HSV-1, but not MV, induced NEAT1v2 expression (Figure 5A). Corresponding with this, HSV-1 infection induced excess formation of paraspeckles without altering the levels of paraspeckle proteins (Figures 5B and 5C and Figure S5A). HSV-1 also induced NEAT1 and the excess formation of paraspeckles in immune cells (Figures S5B and S5C). As expected, MV did not cause excess formation of paraspeckles (Figures S5D and S5F). Influenza virus infection induced excess formation of paraspeckles, even though the paraspeckles were slightly diffuse (Figures S5E and S5G). The *IL8* induction by influenza virus infection was decreased by NEAT1 knockdown (Figures 5D and 5E). In addition, mice infected with influenza virus or HSV-1 induced mNeat1v2 (Figure S5H). These data suggest that the regulation and function of NEAT1 in response to virus infection is evolutionarily conserved.

Cytokines secreted from the cells in response to pathogen infections are known to induce osteoclast differentiation of mouse bone marrow cells (Koide et al., 2010), so bone marrow differentiation can be used to assess the activation of the innate immune response. We therefore carried out the ex vivo experiment using mouse bone marrow cells to get further evidence of involvement of NEAT1 in innate immune response. The supernatant of virus-infected cells with NEAT1 depletion proved less potent for the activation of mouse bone marrow cells than that of virus-infected cells without NEAT1 depletion (Figure 5F). As expected from this result, mouse bone marrow cells showed more activation in response to the supernatant of cells ectopically expressing mNeat1v2 than to the supernatant of control cells (Figure 5F). To strengthen this observation, we performed a similar experiment using immune cells. The chemotaxis of dimethylsulfoxide differentiated HL-60 (DMSO-HL60) cells, neutrophil-like cells, were more activated by the supernatant of virus-infected cells without NEAT1 depletion than by that of virus-infected cells depleted in NEAT1 (Figure 5G). DMSO-HL60 cells showed more activation in response to the supernatant of cells ectopically expressing mNeat1v2 than to the supernatant of control

(C) Schematic of the 5′ region of the *IL8* gene. Fine line, medium gray line, thick black line, and hatched line box indicate the promoter region, 5′ UTR, ORF, and SFPQ binding sequence, respectively. Gray lines below the *IL8* gene indicate the regions amplified by the qPCR primer sets for chromatin immunoprecipitation (ChIP) analysis. The panel at the bottom of the figure shows the conservation score of sequences along the 5′ region of the *IL8* gene. Transcriptional regulatory elements along this region are indicated.

(D) HeLa TO cells stimulated with (black bar) and without (white bar) poly I:C were subjected to ChIP of the 5′ region of the *IL8* gene. Error bars indicate the errors of two replicates.

(E) ChIP of the 5′ region of the *IL8* gene of HeLa TO cells transfected with either mock vector (white bar), pCMV-mNeat1v1 (gray bar), or pCMV-mNeat1v2 (black bar). Error bars indicate the errors of two replicates.

(F) The amount of NEAT1v2 coimmunoprecipitated with endogenous SFPQ was determined by RT-qPCR analysis. The relative amount of NEAT1v2 isolated by anti-SFPQ antibody was normalized to that isolated by the control IgG. Black and white bars indicate the relative amount of NEAT1v2 isolated from cells treated with or without poly I:C, respectively. Values represent the mean ± SD (*$p < 0.01$, Student's t test).

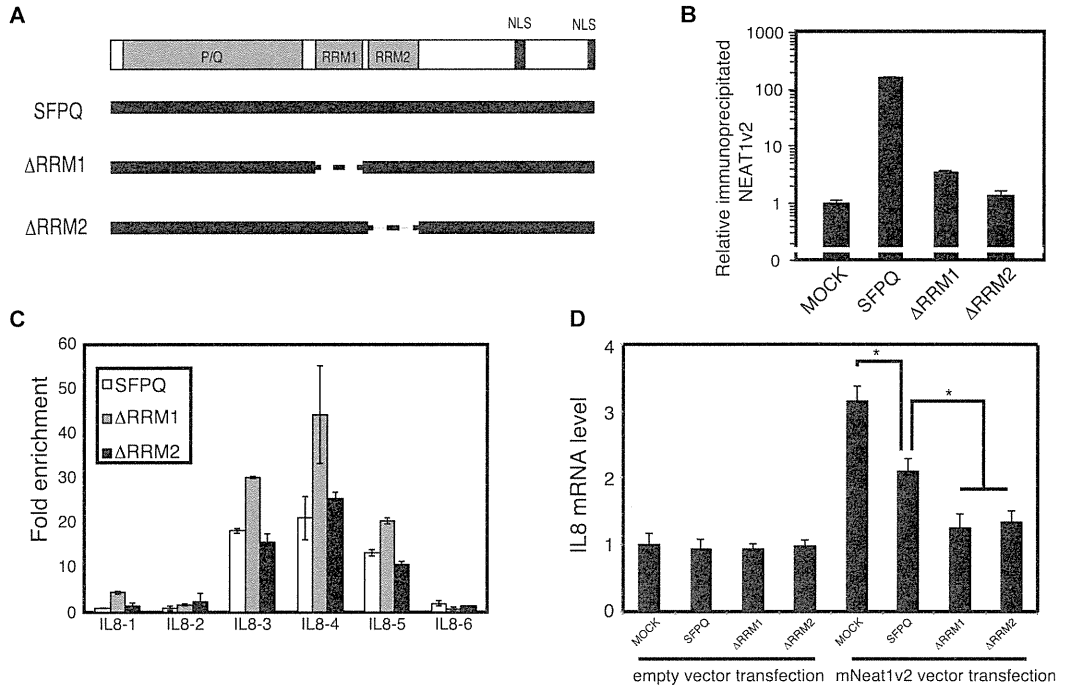

(legend on next page)

cells (Figure 5G). These results indicate that NEAT1 is induced by certain viruses and that it plays an important role in the innate immune response to viral infection.

DISCUSSION

In this study, we report that NEAT1 is induced by viral infection as well as by poly I:C stimulation. Moreover, we found that the stimulus-responsive cooperative action of NEAT1 and SFPQ regulates the expression of genes including those of antiviral factors such as cytokines (Figure 6).

The mechanisms of action of lncRNAs are diverse, ranging from guidance of the chromatin-modifying complexes to acting as "molecular sponges" for the capture of microRNAs (Mercer et al., 2009; Wang and Chang, 2011). For example, lncRNA GAS5 interacts directly with the DNA-binding domain of the glucocorticoid receptor, preventing the receptor from binding to its DNA response element, thereby in effect acting as a molecular decoy (Kino et al., 2010; Tani et al., 2013). LncRNA MALAT1 and TUG1 promote the relocalization of growth-control genes between nuclear subcompartments and thereby regulate gene expression during growth signaling (Yang et al., 2011). More recently, Hirose et al. reported the role of NEAT1 in transcriptional regulation through the sequestering of SFPQ from the RNA-specific adenosine deaminase B2 (ADARB2) gene in response to proteasome inhibition (Hirose et al., 2014). In contrast to our result, the authors showed the importance of the NEAT1-SFPQ interaction in the reduction of ADARB2 transcription. Thus, the NEAT1-SFPQ interaction plays roles in both repression and activation of genes, likely depending on the context of the promoter sequence or interplay with other transcriptional factor(s).

Although there are increasing data that show that lncRNA-protein interactions appear to function in the regulation of gene expression patterns, the identification of the critical short RNA sequences in functional lncRNAs was limited. We attempted to determine the minimal short RNA region in NEAT1 with which SFPQ interacts. We extrapolated the SFPQ binding region in NEAT1v2 by employing the data set of a recent study that systematically identified the RNA sequence motifs recognized by SFPQ (Ray et al., 2013). The potential SFPQ binding sequences were identified in a broad region of NEAT1v2 (Figure S4A). Among these potential SFPQ binding sequences, we showed that two NEAT1 sequences, containing highly ranked SFPQ-binding RNA sequences reported by Ray et al., bound directly and specifically to SFPQ (Figures S4B–S4D). These SFPQ-binding NEAT1 RNAs did not affect the level of mNeat1v2-mediated IL8 transcription (Figure S4E), corresponding to the result in Figure 4. It has been reported that certain RNA binding proteins require a long length of the RNA binding partner to achieve adequate protein function. For instance, polycomb repressive complex 2 (PRC2), containing an RNA binding protein, shows higher affinity to longer partner lncRNAs (Davidovich et al., 2013). In a similar manner as PRC2, SFPQ may require a long NEAT1 RNA sequence (~15 kb) to exert proper function, namely releasing from the IL8 promoter as described in this research.

In this report, we focused on the role of NEAT1 in host antiviral response. However, NEAT1 is also likely to regulate the expression of viral genes themselves, because several paraspeckle proteins are known to play a role in viral replication or viral gene expression (Oakland et al., 2013; Zhang et al., 2008; Zolotukhin et al., 2003). It is reasonable to assume that NEAT1-mediated remodeling of the nuclear localization of paraspeckle proteins directly affects viral replication and/or viral gene expression. Indeed, a recent report observed that NEAT1 modulates HIV-I replication by affecting the nucleus-to-cytoplasm export of Rev-dependent instability element-containing HIV-I mRNAs (Zhang et al., 2013). They showed that MALAT1 lncRNA localized in nuclear speckles was also induced by HIV infection. However, MALAT1 was not induced by poly I:C treatment and virus infections (Figure S5I). Thus, the induction of NEAT1 in response to viral infection may be a more general phenomenon than MALAT1 induction. In the present work, we propose that the TLR3-p38 pathway contributes to the induction of NEAT1 in response to poly I:C stimulation. Since poly I:C generally simulates the action of dsRNAs produced by viral infection, we speculate that viral infections also induce NEAT1 through the TLR3-p38 pathway. Analysis of the paraspeckle entities will reveal a novel mode(s) of viral replication and will contribute to a deeper understanding of viral life cycles and to the development of antiviral drugs.

The transcriptional regulation of cytokine genes in response to pathogen infection lies at the heart of immune response research. In terms of the transcriptional activation of the *IL8* gene, NF-κB, AP-1, and C/EBP play an important role. In this report, we have added another layer to knowledge of the transcriptional regulation system by uncovering the cooperative action between nuclear lncRNA and transcriptional regulator. The

Figure 4. Structure-Function Relationship Study of SFPQ and NEAT1

(A) Schematic diagrams of SFPQ deletion mutants. P/Q, RRM, and NLS indicate the P/Q domain, RNA binding motif, and nuclear localization signal, respectively. Dashed lines indicate the deleted regions in the mutant SFPQs.

(B) RNA immunoprecipitation experiment of the SFPQs. Cells transfected with plasmids expressing FLAG-tagged SFPQs were subjected to immunoprecipitation using an anti-FLAG antibody (clone M2; Sigma). The amounts of NEAT1v2 coimmunoprecipitated with the indicated FLAG-tagged SFPQs were determined by RT-qPCR analysis. The relative amounts of NEAT1v2 isolated by the anti-FLAG antibody were normalized to that isolated by the control IgG.

(C) ChIP analysis of the 5′ region of the *IL8* gene in HeLa TO cells transfected with plasmids expressing the indicated FLAG-tagged SFPQs. The relative amounts of IL8 promoter region DNA isolated by the anti-FLAG antibody were normalized to that isolated by the control IgG. Error bars indicate the errors of two replicate experiments.

(D) IL8 mRNA levels in HeLa TO cells transfected with plasmids expressing the indicated SFPQs in the presence or absence of mNeat1v2 expression. Values represent the mean ± SD (*$p < 0.01$, Student's t test).

(E) IL8 mRNA induction activity and SFPQ binding activity of mutant mNeat1s. Black and gray boxes indicate mNeat1v1 and mNeat1v2, respectively. Dashed lines indicate deleted regions. Schematic structures of the mNeat1v2 deletion mutants are indicated on the left. IL8 mRNA induction determined by RT-qPCR and SFPQ binding determined by RNA immunoprecipitation experiments are shown in the center and right, respectively.

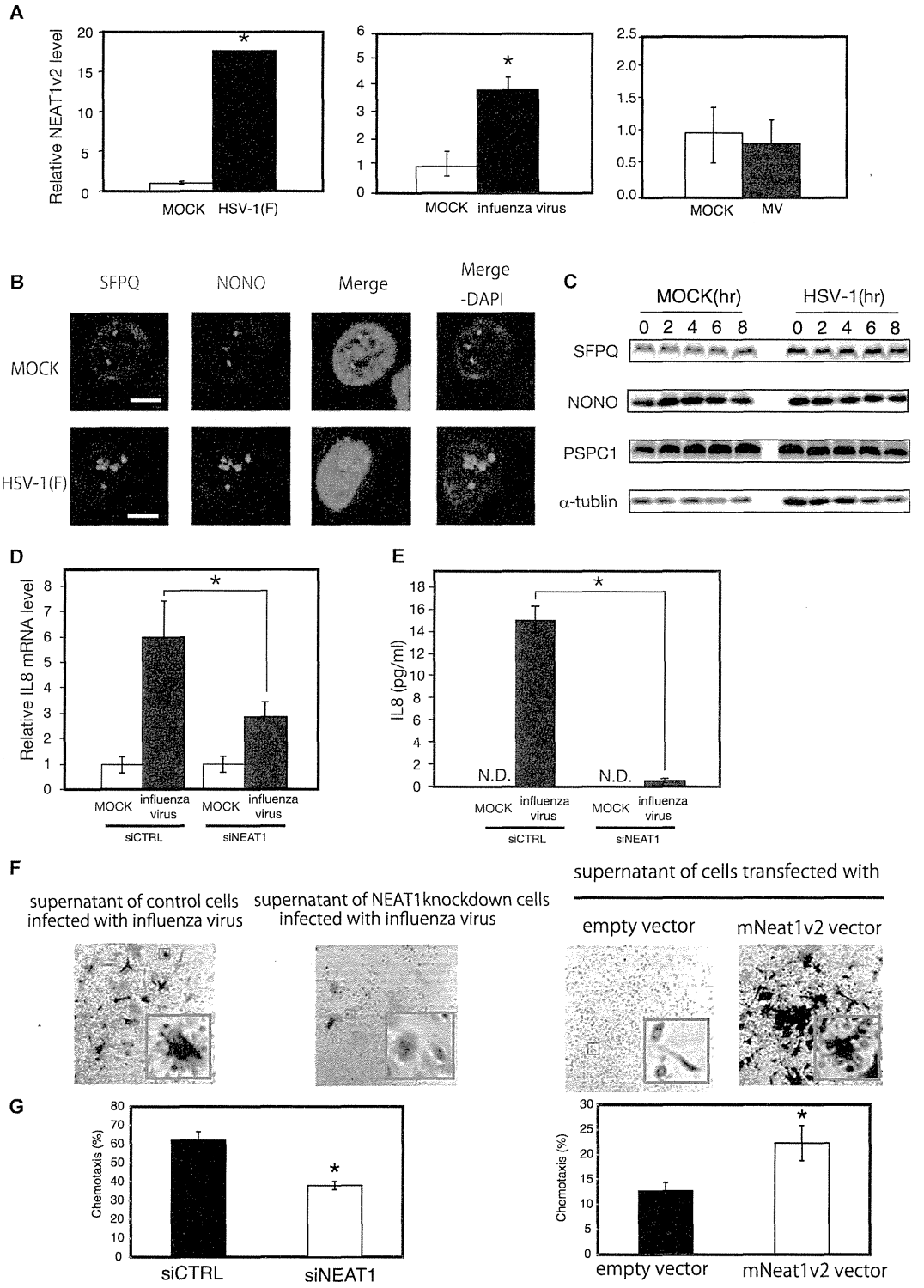

Figure 5. Effect of Viral Infection on NEAT1v2 Induction, Paraspeckle Formation, IL8 Induction, and the Activation of Bone Marrow Cells

(A) NEAT1v2 levels were quantified by RT-qPCR in cells infected with influenza virus, herpes simplex virus 1 (HSV-1), or measles virus (MV). The 18S ribosomal RNA level was used as a normalization control. Values represent the mean ± SD (*$p < 0.01$, Student's t test).

(legend continued on next page)

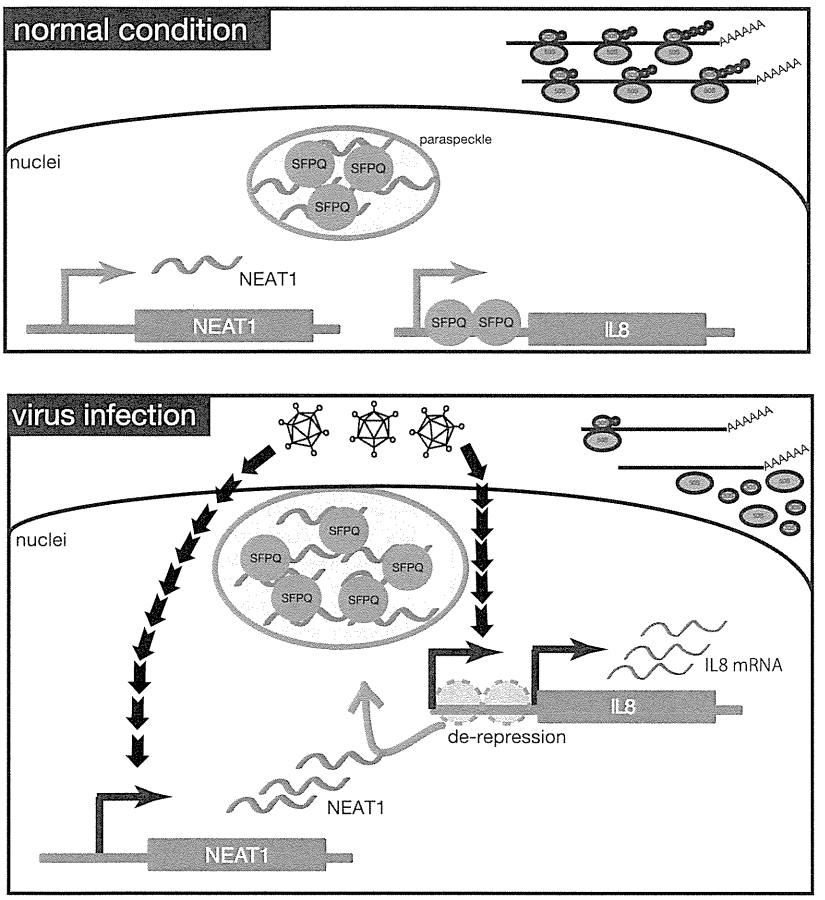

Figure 6. Model of the Transcriptional Regulation of Antiviral Genes Regulated by the Coordinated Action of NEAT1 and Paraspeckle Protein

SFPQs are both located in paraspeckles and bound to gene promoters such as *IL8* under normal conditions. Here, SFPQ represses the transcription of the *IL8* gene. Upon viral infection or poly I:C stimulation, NEAT1 is induced. In the case of poly I:C stimulation, NEAT1 is induced by the TLR3-p38 pathway. NEAT1 induction relocates SFPQ from the *IL8* promoter region and forms excess paraspeckles, consequently activating *IL8* transcription.

high evolutionary conservation of the SFPQ-binding sequence (Figure 3C and Table S3), comparable to that of the AP-1 and C/EBP sites, emphasizes the importance of SFPQ-mediated transcriptional regulation of the *IL8* gene. The established modes of transcriptional activation (NF-κB and so on) and the lncRNA-mediated mode of transcriptional regulation (this study) therefore work in synergy to achieve the precise transcriptional regulation of cytokine genes required during immune response.

SFPQ is known as a multifunctional protein involved in several vital cellular processes, such as pre-mRNA processing. We therefore examined whether NEAT1 controls the function of SFPQ in splicing. We surveyed genes whose splicing patterns were influenced by poly I:C treatment and restored by NEAT1 depletion through a massive sequencing analysis. The poly I:C-induced altered splicing of the *Serine palmitoyltransferase, long chain base subunit 1* gene (increase in variant NM_178324 from 20% to 33%) was restored by NEAT1 depletion (from 28% to 33%) (Figures S2J and S2K). Thus, NEAT1 is also involved in the regulation of SFPQ-mediated splicing regulation.

In this report, there are somewhat superficial nonlinear correlations among NEAT1 expression level, IL8 expression level, SFPQ localization, and paraspeckle size. We think that these superficial nonlinear correlations can be explained by the following interpretations. The *IL8* transcription is regulated by not only NEAT1-SFPQ cooperation, but also the NF-κB pathway. Since both poly I:C treatment and virus infection activate the NF-κB pathway, the effects of these stimuli for IL8 transcription are stronger than that of NEAT1 overexpression, which can only activate SFPQ-mediated IL8 transcription. Therefore, the elevated level of NEAT1v2 (causing excess formation of paraspeckles, but not inducing NF-κB activation) did not lead to a strong induction of IL8 mRNA expression compared with poly I:C treatment or viral infections. Another potential explanation is the presence of multiple functions in SFPQ. Several SFPQ-mediated gene regulation pathways might be involved in the upregulation of IL8 mRNA expression in response to SFPQ depletion. If SFPQ destabilized IL8 mRNA, depletion of SFPQ would increase IL8 mRNA through mRNA stabilization and transcriptional activation. If this was the

(B) HeLa TO cells infected with HSV-1 were subjected to visualization of SFPQ (magenta) and NONO (red) by immunostaining, and of the nuclei by staining with DAPI.

(C) The levels of paraspeckle proteins were analyzed by western blotting at various points post-HSV-1 infection.

(D and E) IL8 mRNA and protein levels were quantified by RT-qPCR and ELISA, respectively, in NEAT1 knockdown cells or control cells infected with (black bars) or without (white bars) influenza virus. Values represent the mean ± SD (*$p < 0.01$, Student's t test).

(F) Microscopic observation of mouse bone marrow cells treated with the supernatants of the indicated cultured cells. The cells were stained using a TRACP and ALP double-stain kit. The red color-stained cells show TRACP activity, indicating the osteoclast differentiation. The blue color-stained cells show ALP activity, indicating the osteoblast differentiation. Values represent the mean ± SD (*$p < 0.01$, Student's t test).

(G) Chemotaxis of DMSO-HL60 cells were assessed by transwell assay. Migrated cells were counted under microscopic observation. Chemotaxis values ((migrated cells / total cells) × 100) represent the means ± SD of three independent experiments. Statistically significant differences ($p < 0.01$) were determined by Student's t test.

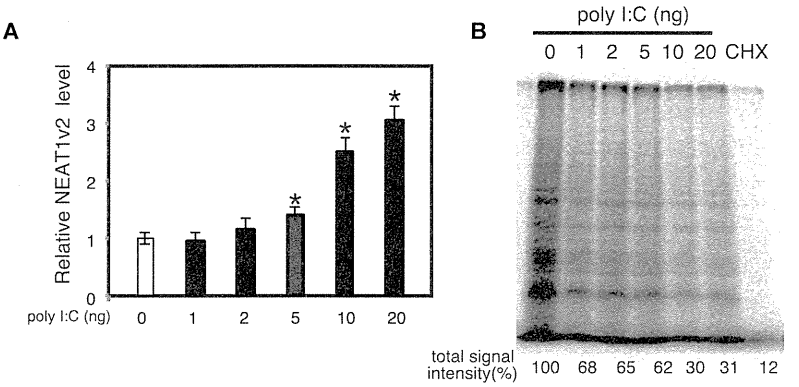

Figure 7. Induction of NEAT1v2 by Poly I:C under Translational Repression

(A) NEAT1v2 levels in cells transfected with the indicated amounts of poly I:C were quantified by RT-qPCR. Values represent the mean ± SD (*$p < 0.01$, Student's t test).

(B) Global translation status of transcription-incompetent HeLa TO cells transfected with the indicated amounts of poly I:C.

(C) NEAT1v2 levels were quantified by RT-qPCR in cells transfected with or without poly I:C under either cycloheximide (CHX; inhibitor for translational elongation) or hippuristanol (HIP; inhibitor for translational initiation) treatments. Values represent the mean ± SD (*$p < 0.01$, Student's t test).

case, depletion of SFPQ would have a stronger effect on the level of IL8 mRNA expression compared with NEAT1 induction-mediated SFPQ modulation. In addition, although NEAT1 should relocate SFPQ from the IL8 promoter, SFPQ proteins are still present in the nucleus. Such SFPQ, even enriched in paraspeckles, might have a certain effect on the IL8 mRNA expression level.

Translation in virus-infected cells is highly repressed (Sonenberg, 1990). For this reason, a translation-independent acute response system is necessary for early immune response. In this regard, the system proposed here is biologically meaningful, because NEAT1 is a noncoding RNA that exerts an effect without need for translation. Indeed, NEAT1 was induced in cells where translation was repressed by poly I:C stimulation (Figure 7). NEAT1v2 was also induced in cells treated with specific translation inhibitors (Figure 7). Translational inhibition did not affect the amounts of paraspeckle proteins (Figure S6B) or the formation of paraspeckles (Figure S6A). These results show that NEAT1v2 exerts an effect under translational repression. We therefore speculate that many other lncRNAs play a role in situations where translation is highly repressed, such as viral infection, heat shock, and hypoxia.

EXPERIMENTAL PROCEDURES

Reagents and Molecular Biological Products

All chemicals were purchased from Wako, unless otherwise stated.

Cell Culture and Transfection

HeLa TO cells (Clontech) and A549 cells (laboratory stock) were grown in Dulbecco's modified Eagle's medium (DMEM), supplemented with 10% fetal bovine serum (FBS) and antibiotics at 37°C in a humidified incubator with 5% CO_2. According to the manufacturer's protocol, cells were transfected with poly I:C or plasmid DNA using Lipofectamine 2000 or Lipofectamine LTX (Invitrogen), respectively. For poly I:C stimulation, cells were seeded into 12-well cell culture plates followed by transfection using the indicated amounts of poly I:C and Lipofectamine 2000. The sequences of the siRNAs are listed in Table S2. siRNAs were transfected into cells using Lipofectamine RNAiMAX (Invitrogen) according to the manufacturer's instructions. Briefly, siRNA duplexes (final concentration 10 nM) and cells were harvested 72 hr posttransfection. RT-qPCR was used to determine whether RNA interference achieved significant depletion of each target sequence.

ChIP Assay

Chromatin was crosslinked with 1% formaldehyde for 10 min at 37°C and then sonicated in lysis buffer (1% SDS, 10 mM EDTA, and 50 mM Tris [pH 8.0], plus protease inhibitor cocktail [Roche]). After centrifugation, 10 μl of the supernatant was used as input, and the remaining lysate was subjected to a ChIP assay using an anti-SFPQ mouse monoclonal antibody (clone B92, Sigma-Aldrich). The primers used to amplify the genes are listed in Table S1.

Viral Infection

HeLa TO cells were seeded into culture plates 1 day before infection and then infected with HSV-1(F) at a multiplicity of infection (moi) of 10. At 72 hr posttransfection with either siRNA or *mNeat1* cDNA, HeLa cells grown in DMEM supplemented with 10% FCS were infected with influenza A virus strain A/WSN/33 at a moi of 3. After incubation for 15 hr, the culture supernatants and total RNAs were collected and subjected to ELISA and RT-qPCR, respectively. MV (Edmonston strain) was propagated in Vero cells grown in DMEM supplemented with 2% FCS. A549 cells were infected with MV at a moi of 0.1.

SUPPLEMENTAL INFORMATION

Supplemental Information includes six figures, four tables, Supplemental Experimental Procedures, and two movies and can be found with this article online at http://dx.doi.org/10.1016/j.molcel.2014.01.009.

AUTHOR CONTRIBUTIONS

K.I., K.S., and N.A. conceived the research strategies, performed experiments, and wrote the paper. N.I., T. Yada, and Y.S. performed bioinformatics analyses. G.A. performed FISH and IF. T. Yamada and T.O. performed FRAP analysis and wrote the manuscript. M. Kumakura, A. Kawaguchi, K.N., A. Kato, Y.K., H.S., M.Y., and C.K. designed the virus infection experiments, performed experiments, and wrote the manuscript. T. Yada analyzed the SFPQ binding region and wrote the paper. K.K., K.I., M. Kobayashi, T.K., and Y.W. designed the microarray analysis, performed experiments, and wrote the manuscript.

ACKNOWLEDGMENTS

We thank Drs. T. Hirose (Hokkaido University) and S. Nakagawa (Riken) for providing mouse Neat1 expression vectors. We thank Drs. Y. Tomari (University of Tokyo), Y. Kumagai (Osaka University), Y.T. Sasaki (AIST), and Y. Hayashi (University of Tokyo) for fruitful discussion and critical comments. We also thank Dr. A. Fox (University of Western Australia), K. Lynch (University of Pennsylvania), A. Matsuzawa (University of Tokyo), and Y. Yoneyama (Chiba University) for providing the mouse monoclonal anti-NONO/p54 antibody, the HIS-SFPQ expression vector, anti-phospho-JNK antibody, and shRNA expression vector to silence RIG-I, respectively. This work was financially supported by the Suzuken Memorial Foundation, the Naito Foundation, Research Fellowship of the Japan Society for the Promotion of Science, Grant-in-Aid for Scientific Research (22310117, 23659050, 23790077), a Grant-in-Aid for Scientific Research on Innovative Areas "Functional machinery for noncoding RNAs," "Genome adaptation," and "Genome science" from the Ministry of Education, Culture, Sports, Science and Technology of Japan, and The Funding Program for World-Leading Innovative R&D on Science and Technology of the Japan Society for the Promotion of Science.

Received: June 6, 2013
Revised: November 8, 2013
Accepted: January 2, 2014
Published: February 6, 2014

REFERENCES

Arpaia, N., and Barton, G.M. (2011). Toll-like receptors: key players in antiviral immunity. Curr Opin Virol *1*, 447–454.

Berghäll, H., Sirén, J., Sarkar, D., Julkunen, I., Fisher, P.B., Vainionpää, R., and Matikainen, S. (2006). The interferon-inducible RNA helicase, mda-5, is involved in measles virus-induced expression of antiviral cytokines. Microbes Infect. *8*, 2138–2144.

Bernard, D., Prasanth, K.V., Tripathi, V., Colasse, S., Nakamura, T., Xuan, Z., Zhang, M.Q., Sedel, F., Jourdren, L., Coulpier, F., et al. (2010). A long nuclear-retained non-coding RNA regulates synaptogenesis by modulating gene expression. EMBO J. *29*, 3082–3093.

Carninci, P., Kasukawa, T., Katayama, S., Gough, J., Frith, M.C., Maeda, N., Oyama, R., Ravasi, T., Lenhard, B., Wells, C., et al.; FANTOM Consortium; RIKEN Genome Exploration Research Group and Genome Science Group (Genome Network Project Core Group) (2005). The transcriptional landscape of the mammalian genome. Science *309*, 1559–1563.

Chen, L.L., and Carmichael, G.G. (2009). Altered nuclear retention of mRNAs containing inverted repeats in human embryonic stem cells: functional role of a nuclear noncoding RNA. Mol. Cell *35*, 467–478.

Chen, L.L., and Carmichael, G.G. (2010). Decoding the function of nuclear long non-coding RNAs. Curr. Opin. Cell Biol. *22*, 357–364.

Clemson, C.M., Hutchinson, J.N., Sara, S.A., Ensminger, A.W., Fox, A.H., Chess, A., and Lawrence, J.B. (2009). An architectural role for a nuclear noncoding RNA: NEAT1 RNA is essential for the structure of paraspeckles. Mol. Cell *33*, 717–726.

Davidovich, C., Zheng, L., Goodrich, K.J., and Cech, T.R. (2013). Promiscuous RNA binding by Polycomb repressive complex 2. Nat. Struct. Mol. Biol. *20*, 1250–1257.

Fox, A.H., and Lamond, A.I. (2010). Paraspeckles. Cold Spring Harb. Perspect. Biol. *2*, a000687.

Guillot, L., Le Goffic, R., Bloch, S., Escriou, N., Akira, S., Chignard, M., and Si-Tahar, M. (2005). Involvement of toll-like receptor 3 in the immune response of lung epithelial cells to double-stranded RNA and influenza A virus. J. Biol. Chem. *280*, 5571–5580.

Gupta, R.A., Shah, N., Wang, K.C., Kim, J., Horlings, H.M., Wong, D.J., Tsai, M.C., Hung, T., Argani, P., Rinn, J.L., et al. (2010). Long non-coding RNA HOTAIR reprograms chromatin state to promote cancer metastasis. Nature *464*, 1071–1076.

Guttman, M., Amit, I., Garber, M., French, C., Lin, M.F., Feldser, D., Huarte, M., Zuk, O., Carey, B.W., Cassady, J.P., et al. (2009). Chromatin signature reveals over a thousand highly conserved large non-coding RNAs in mammals. Nature *458*, 223–227.

Hirose, T., Virnicchi, G., Tanigawa, A., Naganuma, T., Li, R., Kimura, H., Yokoi, T., Nakagawa, S., Bénard, M., Fox, A.H., and Pierron, G. (2014). NEAT1 long noncoding RNA regulates transcription via protein sequestration within subnuclear bodies. Mol. Biol. Cell *25*, 169–183.

Hoffmann, E., Dittrich-Breiholz, O., Holtmann, H., and Kracht, M. (2002). Multiple control of interleukin-8 gene expression. J. Leukoc. Biol. *72*, 847–855.

Huarte, M., and Rinn, J.L. (2010). Large non-coding RNAs: missing links in cancer? Hum. Mol. Genet. *19* (R2), R152–R161.

Hutchinson, J.N., Ensminger, A.W., Clemson, C.M., Lynch, C.R., Lawrence, J.B., and Chess, A. (2007). A screen for nuclear transcripts identifies two linked noncoding RNAs associated with SC35 splicing domains. BMC Genomics *8*, 39.

Iacobazzi, V., Infantino, V., Costanzo, P., Izzo, P., and Palmieri, F. (2005). Functional analysis of the promoter of the mitochondrial phosphate carrier human gene: identification of activator and repressor elements and their transcription factors. Biochem. J. *391*, 613–621.

Kapranov, P., Willingham, A.T., and Gingeras, T.R. (2007). Genome-wide transcription and the implications for genomic organization. Nat. Rev. Genet. *8*, 413–423.

Kawai, T., and Akira, S. (2010). The role of pattern-recognition receptors in innate immunity: update on Toll-like receptors. Nat. Immunol. *11*, 373–384.

Kino, T., Hurt, D.E., Ichijo, T., Nader, N., and Chrousos, G.P. (2010). Noncoding RNA gas5 is a growth arrest- and starvation-associated repressor of the glucocorticoid receptor. Sci. Signal. *3*, ra8.

Koide, M., Kinugawa, S., Takahashi, N., and Udagawa, N. (2010). Osteoclastic bone resorption induced by innate immune responses. Periodontol. 2000 *54*, 235–246.

Lafaille, F.G., Pessach, I.M., Zhang, S.Y., Ciancanelli, M.J., Herman, M., Abhyankar, A., Ying, S.W., Keros, S., Goldstein, P.A., Mostoslavsky, G., et al. (2012). Impaired intrinsic immunity to HSV-1 in human iPSC-derived TLR3-deficient CNS cells. Nature *491*, 769–773.

Mao, Y.S., Zhang, B., and Spector, D.L. (2011). Biogenesis and function of nuclear bodies. Trends Genet. *27*, 295–306.

Mercer, T.R., Dinger, M.E., and Mattick, J.S. (2009). Long non-coding RNAs: insights into functions. Nat. Rev. Genet. *10*, 155–159.

Miyagawa, R., Tano, K., Mizuno, R., Nakamura, Y., Ijiri, K., Rakwal, R., Shibato, J., Masuo, Y., Mayeda, A., Hirose, T., and Akimitsu, N. (2012). Identification of cis- and trans-acting factors involved in the localization of MALAT-1 noncoding RNA to nuclear speckles. RNA *18*, 738–751.

Mizutani, R., Wakamatsu, A., Tanaka, N., Yoshida, H., Tochigi, N., Suzuki, Y., Oonishi, T., Tani, H., Tano, K., Ijiri, K., et al. (2012). Identification and characterization of novel genotoxic stress-inducible nuclear long noncoding RNAs in mammalian cells. PLoS ONE *7*, e34949.

Naganuma, T., and Hirose, T. (2013). Paraspeckle formation during the biogenesis of long non-coding RNAs. RNA Biol. *10*, 456–461.

Naganuma, T., Nakagawa, S., Tanigawa, A., Sasaki, Y.F., Goshima, N., and Hirose, T. (2012). Alternative 3′-end processing of long noncoding RNA initiates construction of nuclear paraspeckles. EMBO J. *31*, 4020–4034.

Nakagawa, S., and Hirose, T. (2012). Paraspeckle nuclear bodies—useful uselessness? Cell. Mol. Life Sci. *69*, 3027–3036.

Oakland, T.E., Haselton, K.J., and Randall, G. (2013). EWSR1 binds the hepatitis C virus cis-acting replication element and is required for efficient viral replication. J. Virol. *87*, 6625–6634.

Peng, R., Dye, B.T., Pérez, I., Barnard, D.C., Thompson, A.B., and Patton, J.G. (2002). PSF and p54nrb bind a conserved stem in U5 snRNA. RNA *8*, 1334–1347.

Ponting, C.P., Oliver, P.L., and Reik, W. (2009). Evolution and functions of long noncoding RNAs. Cell *136*, 629–641.

Prasanth, K.V., and Spector, D.L. (2007). Eukaryotic regulatory RNAs: an answer to the 'genome complexity' conundrum. Genes Dev. *21*, 11–42.

Rathinam, V.A., and Fitzgerald, K.A. (2011). Cytosolic surveillance and antiviral immunity. Curr Opin Virol *1*, 455–462.

Ray, D., Kazan, H., Cook, K.B., Weirauch, M.T., Najafabadi, H.S., Li, X., Gueroussov, S., Albu, M., Zheng, H., Yang, A., et al. (2013). A compendium of RNA-binding motifs for decoding gene regulation. Nature *499*, 172–177.

Saha, S., Murthy, S., and Rangarajan, P.N. (2006). Identification and characterization of a virus-inducible non-coding RNA in mouse brain. J. Gen. Virol. *87*, 1991–1995.

Sasaki, Y.T., Ideue, T., Sano, M., Mituyama, T., and Hirose, T. (2009). MENepsilon/beta noncoding RNAs are essential for structural integrity of nuclear paraspeckles. Proc. Natl. Acad. Sci. USA *106*, 2525–2530.

Scaria, V., and Pasha, A. (2012). Long Non-Coding RNAs in Infection Biology. Front Genet *3*, 308.

Sonenberg, N. (1990). Measures and countermeasures in the modulation of initiation factor activities by viruses. New Biol. *2*, 402–409.

Song, X., Sui, A., and Garen, A. (2004). Binding of mouse VL30 retrotransposon RNA to PSF protein induces genes repressed by PSF: effects on steroidogenesis and oncogenesis. Proc. Natl. Acad. Sci. USA *101*, 621–626.

Sunwoo, H., Dinger, M.E., Wilusz, J.E., Amaral, P.P., Mattick, J.S., and Spector, D.L. (2009). MEN epsilon/beta nuclear-retained non-coding RNAs are up-regulated upon muscle differentiation and are essential components of paraspeckles. Genome Res. *19*, 347–359.

Tani, H., Mizutani, R., Salam, K.A., Tano, K., Ijiri, K., Wakamatsu, A., Isogai, T., Suzuki, Y., and Akimitsu, N. (2012). Genome-wide determination of RNA stability reveals hundreds of short-lived noncoding transcripts in mammals. Genome Res. *22*, 947–956.

Tani, H., Torimura, M., and Akimitsu, N. (2013). The RNA degradation pathway regulates the function of GAS5 a non-coding RNA in mammalian cells. PLoS ONE *8*, e55684.

Tano, K., Mizuno, R., Okada, T., Rakwal, R., Shibato, J., Masuo, Y., Ijiri, K., and Akimitsu, N. (2010). MALAT-1 enhances cell motility of lung adenocarcinoma cells by influencing the expression of motility-related genes. FEBS Lett. *584*, 4575–4580.

Thompson, M.R., Kaminski, J.J., Kurt-Jones, E.A., and Fitzgerald, K.A. (2011). Pattern recognition receptors and the innate immune response to viral infection. Viruses *3*, 920–940.

Urban, R.J., Bodenburg, Y., Kurosky, A., Wood, T.G., and Gasic, S. (2000). Polypyrimidine tract-binding protein-associated splicing factor is a negative regulator of transcriptional activity of the porcine p450scc insulin-like growth factor response element. Mol. Endocrinol. *14*, 774–782.

Wang, K.C., and Chang, H.Y. (2011). Molecular mechanisms of long noncoding RNAs. Mol. Cell *43*, 904–914.

Yang, L., Lin, C., Liu, W., Zhang, J., Ohgi, K.A., Grinstein, J.D., Dorrestein, P.C., and Rosenfeld, M.G. (2011). ncRNA- and Pc2 methylation-dependent gene relocation between nuclear structures mediates gene activation programs. Cell *147*, 773–788.

Yoon, J.H., Abdelmohsen, K., and Gorospe, M. (2013). Posttranscriptional Gene Regulation by Long Noncoding RNA. J. Mol. Biol. *425*, 3723–3730.

Zhang, S.Y., Jouanguy, E., Ugolini, S., Smahi, A., Elain, G., Romero, P., Segal, D., Sancho-Shimizu, V., Lorenzo, L., Puel, A., et al. (2007). TLR3 deficiency in patients with herpes simplex encephalitis. Science *317*, 1522–1527.

Zhang, W., Zhang, X., Tian, C., Wang, T., Sarkis, P.T., Fang, Y., Zheng, S., Yu, X.F., and Xu, R. (2008). Cytidine deaminase APOBEC3B interacts with heterogeneous nuclear ribonucleoprotein K and suppresses hepatitis B virus expression. Cell. Microbiol. *10*, 112–121.

Zhang, Q., Chen, C.Y., Yedavalli, V.S., and Jeang, K.T. (2013). NEAT1 long noncoding RNA and paraspeckle bodies modulate HIV-1 posttranscriptional expression. MBio *4*, e00596–e12.

Zolotukhin, A.S., Michalowski, D., Bear, J., Smulevitch, S.V., Traish, A.M., Peng, R., Patton, J., Shatsky, I.N., and Felber, B.K. (2003). PSF acts through the human immunodeficiency virus type 1 mRNA instability elements to regulate virus expression. Mol. Cell. Biol. *23*, 6618–6630.

Biochemical and Biophysical Research Communications 443 (2014) 975–979

Contents lists available at ScienceDirect

Biochemical and Biophysical Research Communications

journal homepage: www.elsevier.com/locate/ybbrc

Involvement of the N-terminal portion of influenza virus RNA polymerase subunit PB1 in nucleotide recognition

Nguyen Trong Binh [b], Chitose Wakai [a], Atsushi Kawaguchi [a,b], Kyosuke Nagata [c,*]

[a] Department of Infection Biology, Faculty of Medicine, University of Tsukuba, 1-1-1 Tennodai, Tsukuba 305-8575, Japan
[b] Graduate School of Comprehensive Human Sciences, University of Tsukuba, 1-1-1 Tennodai, Tsukuba 305-8575, Japan
[c] University of Tsukuba, 1-1-1 Tennodai, Tsukuba 305-8575, Japan

ARTICLE INFO

Article history:
Received 26 November 2013
Available online 19 December 2013

Keywords:
Influenza
Nucleotide recognition
Resistant mutant
Ribavirin

ABSTRACT

The influenza virus PB1 protein functions as a catalytic subunit of the viral RNA-dependent RNA polymerase and contains the highly conserved motifs of RNA-dependent RNA polymerases together with putative nucleotide-binding sites. PB1 also binds to viral genomic RNAs and its replicative intermediates through the promoter regions. The detail function and interplay between functional domains are not clarified although a part of structures and functions of PB1 have been clarified. In this study, we analyzed the function of PB1 subunit in the sense of nucleotide recognition using ribavirin, which is a nucleoside analog and inhibits viral RNA synthesis of many RNA viruses including influenza virus. We screened ribavirin-resistant PB1 mutants from randomly mutated PB1 cDNA library using a mini-replicon assay, and we identified a single mutation at the amino acid position 27 of PB1 as an important residue for the nucleotide recognition.

1. Introduction

Influenza A virus belongs to the family of *Orthomyxoviridae*. Its genome consists of eight-segmented and single-stranded RNAs of negative polarity (vRNA). Each segment is encapsidated by nucleoprotein (NP) and associated with viral RNA polymerases to form viral ribonucleoprotein (vRNP) complexes. The vRNP complex is a basic unit for both transcription and replication [1]. The viral mRNA transcription is initiated using capped oligonucleotide as a primer. The elongation of mRNA chain proceeds until the viral polymerase reaches oligo U sequence present near the 5′-terminus of vRNA, and then the poly A tail is added by the viral RNA polymerase. In the viral genome replication, full-length cRNA (complementary RNA to vRNA) is generated from vRNA in a primer-independent manner, and progeny vRNAs are amplified from cRNA by the viral RNA polymerase. The viral RNA polymerase consists of PB1, PB2, and PA. PB1 functions as a catalytic subunit and the assembly core of the viral RNA polymerase [2–7]. PA is genetically found to be involved in the replication process and the polymerase assembly [8] and have the endonuclease activity [9–12]. PB2 is responsible for the recognition and binding of the cap structure [1,13–16].

The 14 amino acids residues from the N-terminus of PB1 interact with PA [4–7,17–20], while the C-terminal region of PB1 between amino acid (a.a.) positions 678–757 interacts with PB2 [4–6,21,22]. PB1 contains the motifs highly conserved among RNA-dependent RNA polymerases [2]. There are two putative nucleotide-binding sites between a.a. positions 179–297 and 458–519 [23,24]. Moreover, the N-terminal (a.a. positions 1–83) and C-terminal (a.a. positions 494–757) regions of PB1 are suggested to interact with the vRNA promoter [25]. In addition, the a.a. positions 249–254 of PB1 is important for the vRNA binding, and Phe251 (when the number indicates the amino acid position) and Phe254 are essential for this binding [26]. It is also reported that the regions between a.a. positions 1–139 and 267–493 bind to the cRNA promoter [27].

Ribavirin (1-β-D-ribofusanosyl-1,2,4-triazole-3-carboxamide, also known as Virazole) is a synthetic purine nucleoside analogue first synthesized by Sidwell et al. in 1972 [28]. It is phosphorylated by cellular adenosine kinases into ribavirin monophosphate, diphosphate, and triphosphate (RMP, RDP, and RTP, respectively) [29,30]. Ribavirin inhibits various RNA-dependent RNA polymerases such as those from influenza virus [31], vesicular stomatitis virus [32], La Crosse virus [33], Hantaan virus [34], Foot and mouth disease virus [35], West Nile virus [36], Andes virus [37], and Hepatitis C virus [38]. In contrast, ribavirin does not inhibit cellular RNA polymerase I, RNA polymerase II, and poly (A) polymerase [39]. Ribavirin inhibits the inosine monophosphate dehydrogenase, so that the *de novo* synthesis of purine nucleosides is interrupted [40]. Further, it

* Corresponding author. Address: Department of Infection Biology, Faculty of Medicine, University of Tsukuba, 1-1-1 Tennodai, Tsukuba 305-8575, Japan. Fax: +81 29 853 3233.
E-mail address: knagata@md.tsukuba.ac.jp (K. Nagata).

0006-291X/$ - see front matter © 2013 Elsevier Inc. All rights reserved.
http://dx.doi.org/10.1016/j.bbrc.2013.12.071